Phase Transform Time Delay Estimation to Counteract Spectral Haystacking Effects in Jet Exhaust Flow Measurements

Kevin Alexander Silas

Thesis submitted to the faculty of the Virginia Polytechnic Institute and State University in partial fulfillment of the requirements for the degree of

Master of Science
In
Mechanical Engineering

Co-chair: Wing F. Ng
Co-chair: Kevin T. Lowe
Joseph W. Meadows

August 13, 2021
Blacksburg, VA

Keywords: acoustics, phase transform, Hartmann, coaxial bypass, shear layer, haystacking

Phase Transform Time Delay Estimation to Counteract Haystacking Effects in Jet Exhaust Flow Measurements

Kevin Alexander Silas

Academic Abstract

This study determined a superior data processing technique for correlating an acoustic signal passing through a subsonic jet engine exhaust in order to estimate the traversal time of the signal. Thrust measurement is possible with enough time delay estimates across different portions of the exhaust. This preliminary study did not take the full array of data necessary to measure thrust, but did validate key aspects of the measurement process. The turbulent shear layers of the exhaust spectrally broaden the signal, creating the appearance of spectral "haystacks", making traditional correlation methods unworkable. An experiment was performed to evaluate the ability of a novel sound source to produce a signal from which a reliable and precise time delay estimate could be found. The test apparatus was installed on either side of a Honeywell TFE731-2 turbofan research engine exhaust cone, with the source and receivers placed near the jet exit plane. The signal was then directed across the jet exhaust. This flow environment is considered an extreme challenge for accurate acoustic signal propagation. A key contribution of this paper is the determination that the Phase Transform processor of the Generalized Cross-Correlation (GCC) method produces the most reliable time delay estimates, for the given signal and flow conditions. Several alternative time delay estimators and GCC processors were examined and evaluated on this data. A proposed explanation is provided for why this time delay estimation technique produces the most accurate results, as well as explanations for why the technique became less reliable as the flow environment became more challenging, with an observed 22% anomalous TDE selection rate for the N_{1Corr} = 60% and N_{1Corr} = 70% conditions combined, versus only 6% for the idle and N_{1Corr} = 50% conditions combined. This paper also details the development and first use of a novel acoustic source that produces a two-tone narrowband signal emanating from a single point – the dual Hartmann generator.

Phase Transform Time Delay Estimation to Counteract Haystacking Effects in Jet Exhaust Flow Measurements

Kevin Alexander Silas

General Audience Abstract

This study builds on a Computational Tomography (CT) technique that uses an acoustic signal and an array of receivers to measure the velocity and temperature of a gas flow field. In particular, the velocity and temperature field tested involves multiple turbulent and disruptive elements, requiring a loud and specifically designed signal. As such, a novel acoustic signal generator, the dual Hartmann generator, was designed that is both loud and produces a specific two-toned signal. The key contribution of the study was to process the data, comparing the sets of transmitted and received signals, in order to estimate the time delay amongst receiver pairs – a key input in the CT method. Traditional cross-correlation methods were inadequate, and multiple alternatives were evaluated. The Phase Transform (PHAT) technique showed the most promise, and an explanation is given for why this technique is most suitable for this type of signal.

Acknowledgements

The support given to me by my wife, Molly over the course of my graduate school career has been immense and nothing short of heroic. I thank her with my whole heart.

I would like to thank and acknowledge my collaborators on this work. Dr. Raul Otero, for getting me up to speed on the work and setting up a wonderful foundation for this research. John Gillespie for all his support for our team and me personally over the years to plan and execute our experimental visions, with particular thanks to turning sketches and dimensions into the working dual Hartmann prototype. And to George Boggs, collaborator on a large part of this project, who helped make sense of all the data, and who never hesitated to listen to a new avenue of thought.

I would also like to thank my co-advisors, Dr. Ng, and Dr. Lowe. Dr. Ng, for all the support and patience over the years, thank you. Dr. Lowe, thank you for your support and technical advice, particularly when you would provide a new direction to explore.

Kevin Silas

August, 2021

Table of Contents

List of Figures

List of Tables

Introduction and Structure

The primary objective of this work has been to extend the application of acoustic non-intrusive flow measurement in high sub-sonic conditions and, in particular, acoustic tomography to the scale of a coaxial bypass jet engine. The work of Otero et al. [2-5] has been in large part a basis of this present work. Scaling the measurement methods to larger engine diameters has presented challenges that have been addressed in part by this thesis. The author has put forth considerable effort to research and design a prototype of a new acoustic source that was tested in both a benchtop setting and during a jet engine application validation test. Furthermore, the author has put forth considerable effort developing a data processing approach that is tailored to this particular application.

Structure

This thesis is presented in a manuscript format, with the bulk of the technical content distilled into a manuscript which is intended for an archival technical journal. The paper focuses on the signal processing approach that was researched, applied, and refined for the new acoustic source signal passing through a jet engine exhaust flow. In addition, the author of this thesis is a co-author on several related works already appearing in the archival literature, including [5] (acoustic tomography on a 2" hot jet), where he contributed experimental testing support and assistance in the post-processing of the data; [12] (dual Hartmann generator acoustic and hydrodynamic study), where he contributed experimental testing support and acoustic data analysis; and in another M.S. thesis, [27] (Pneumatic Horn Tomography), where he contributed to the planning and execution of experimental testing, data processing, and analysis of results. The remainder of the thesis consists of appendices that detail several aspects of the work in greater depth. The paper as presented here will include reference to these appendix sections as appropriate.

Appendix A is a detailed look into how the new acoustic source, the dual Hartmann generator, was developed – complete with literature inspiration, design parameters decisions, and notes on the operation of the device. **Appendix B** provides notes and discussion of the time delay estimation processing research, which methods were investigated but not discussed by the paper, and further notes on the GCC method. **Appendix C** contains additional figures showing comparsions of different GCC processors as applied to the acoustic measurements. **Appendix D** is a derivation of the expected time delay values under ambient conditions, as well as a comparison to measured values. **Appendix E** contains copies of MATLAB code employed to process the data.

TFE731 Engine Experiment Paper

Phase Transform Time Delay Estimation to Counteract Spectral Haystacking Effects in Jet Exhaust Flow Measurements

Kevin Silas[1], George Boggs[1], Todd Lowe[2], and Wing Ng[3]

E-mail: kasilas@vt.edu

Abstract

This study determined a superior data processing technique for correlating an acoustic signal passing through a subsonic jet engine exhaust in order to estimate the traversal time of the signal. Thrust measurement is possible with enough time delay estimates across different portions of the exhaust. This preliminary study did not take the full array of data necessary to measure thrust, but did validate key aspects of the measurement process. The turbulent shear layers of the exhaust spectrally broaden the signal, creating the appearance of spectral "haystacks", making traditional correlation methods unworkable. An experiment was performed to evaluate the ability of a novel sound source to produce a signal from which a reliable and precise time delay estimate could be found. The test apparatus was installed on either side of a Honeywell TFE731-2 turbofan research engine exhaust cone, with the source and receivers placed near the jet exit plane. The signal was then directed across the jet exhaust. This flow environment is considered an extreme challenge for accurate acoustic signal propagation. A key contribution of this paper is the determination that the Phase Transform processor of the Generalized Cross-Correlation (GCC) method produces the most reliable time delay estimates, for the given signal and flow conditions. Several alternative time delay estimators and GCC processors were examined and evaluated on this data. A proposed explanation is provided for why this time delay estimation technique produces the most accurate results, as well as explanations for why the technique became less reliable as the flow environment became more challenging, with an observed 22% anomalous TDE selection rate for the N_{1Corr} = 60% and N_{1Corr} = 70% conditions combined, versus only 6% for the idle and N_{1Corr} = 50% conditions combined.

[1] Graduate Research Assistant
[2] Associate Professor, kelowe@vt.edu
[3] Alumni Distinguished Professor, wng@vt.edu

Nomenclature

D_e	- diameter of TFE731-2 engine exhaust exit
D_n	- dual Hartmann generator nozzle diameter
D_r	- dual Hartmann generator resonator diameter
$f_{1,2}$	- dual Hartmann generator fundamental frequencies
f_b	- beat frequency of the dual Hartmann generator ($f_2 - f_1$)
$G_{12}(f)$	- cross-power spectral density (CPSD) between signals $x_1(t)$ and $x_2(t)$
GCC	- **G**eneralized **C**ross-**C**orrelation
L	- axial distance from TFE731 exhaust exit
L_r	- dual Hartmann generator resonator length
Ma	- Mach number
M1,…,10	- microphone number
N_{1Corr}	- Corrected Fan Speed (CFS) of N_1 Turbine
NPR	- **N**ozzle **P**ressure **R**atio
PHAT	- **Pha**se **T**ransform
$\psi(f)$	- processor function applied to the CPSD
$R_{12}(\tau)$	- correlation function between signals $x_1(t)$ and $x_2(t)$
S	- distance between Hartmann generator nozzle and resonator, ‘spacing’
SNR	- **S**ignal-to-**N**oise **R**atio
SPL	- **S**ound **P**ressure **L**evel
τ	- time lag variable
TDE	- **T**ime **D**elay **E**stimate or **T**ime **D**elay **E**stimation
TOF	- **T**ime **O**f **F**light
$x_1(t)$	- received signal at M1
ω	- angular frequency, $= 2\pi f$

1. Introduction

Jet engine manufacturers have a desire to measure parameters of their engines and engine subsystems to make assessments of the health and operation of the engine. This includes measuring exhaust flow parameters, such as thrust and mass flow rate. One way to determine this is by sampling the velocity and temperature to obtain a map of these parameters at the exhaust plane. Traditionally, this has been performed with intrusive temperature and pressure probes inserted into the flow [1]. There are several downsides to this approach, primarily the cost and intrusive nature of the probes. An alternative approach is to measure the flow non-intrusively such as with optics or acoustics.

Much work has been done on the use of acoustic anemometry and thermometry, see especially the work of Otero Jr. et al. [2-5], DeSilva et al. [6], and Wilson and Thomson [7]. Otero Jr. et al. in particular established methodology for resolving velocity and temperature in high subsonic (above Mach 0.3) flows for the first time: a key requirement for the jet engine application. The primary data input for acoustic anemometry and thermometry is accurate estimates of time delay for pairs of two received acoustic signals. Along with spatial information about the receivers, Otero Jr. et al. has developed an algorithm to iteratively reconstruct a full velocity and temperature field map from the time-delay estimates. This Coupled Acoustic Tomography procedure is presented in [4].

As part of an effort to validate and extend the work of Otero Jr. et al. [2-5], a novel acoustic generator was developed. It is based on the nozzle and resonator concept originally discovered by Hartmann and Trolle [8], and known as the Hartmann generator or Hartmann whistle. This new generator aimed to improve upon SNR limitations encountered in past experiments.

A commercial bypass jet engine operating at close to full power produces a challenging, noisy, turbulent medium for passing an acoustic signal. The following experiment characterizes the challenge of sending the signal such that TDE can be performed. The signal is affected by additive noise sources from the engine itself and signal spreading effects from traveling through the large, turbulent shear layers of the jet exhaust.

Due to the intensity of the jet exhaust environment and a new set of signal characteristics, a new approach to signal correlation was necessary. Advanced TDE techniques were investigated based on the work of Knapp and Carter [9]. Ultimately, the PHAT method of the GCC was applied. This paper will show the conditions under which acoustic time of flight can be accurately resolved with reasonable levels of certainty.

2. Background and Literature Review

A. Acoustic Anemometry and Thermometry

The use of acoustic sources and fluid properties to measure distance is well-known (e.g., sonar) [10]. Using acoustics and known distances is also an established way to measure velocity (anemometry) and temperature (thermometry). Anemometry in air, for example, has been used to perform atmospheric tomography by Wilson and Thomson [7]. Desilva et al. [6] developed an acoustic array to perform tomographic thermometry on low-speed (Ma < 0.3), high temperature flow.

These techniques suffered from an inability to capture high subsonic (Ma > 0.3), compressible flow. The work of Otero Jr. et al. [2-5] has extended acoustic anemometry and thermometry into this regime. Each successive paper by Otero Jr. et al. served to extend the technique into a new applicable range, from laboratory small 2” jets to coaxial bypass jets from a full-sized gas turbine propulsion engine.

In [2], Otero Jr. et al. confirmed, using a new combined anemometry and thermometry (CAT) configuration (**Figure 1**), that compressible flow speeds could be measured with low overall error (8.79 m/s RMS error across the measurement span, up to Ma 0.83). In [3], Otero Jr. et al. extended the technique to heated flows and identified limitations with the simplified jet flow model used. To get around these limitations, an acoustic tomography algorithm was developed that takes as input a sufficient number of acoustic ray paths through a flow and iterates to identify flow non-uniformities. In [4], this “Coupled Acoustic Tomography” approach was validated on a 2” heated jet flow as an extension of [3]. An experiment was also performed prior to development of the tomography approach by Otero Jr. et al. to acoustically measure jet engine exhaust flow on a JT15D-1A turbofan engine [5]. This established that CAT could be applied at a larger scale, but the application exposed SNR limitations with the sound source. The spark source employed by Otero Jr. et al. [2-5] was not able to achieve sufficient SNR for the technique to be successful above the 65% of the engine design fan speed condition of the JT15D-1A. In order for the technique validated in ref. [5] to be workable on an engine-scale at high Ma, an improved sound source was necessary.

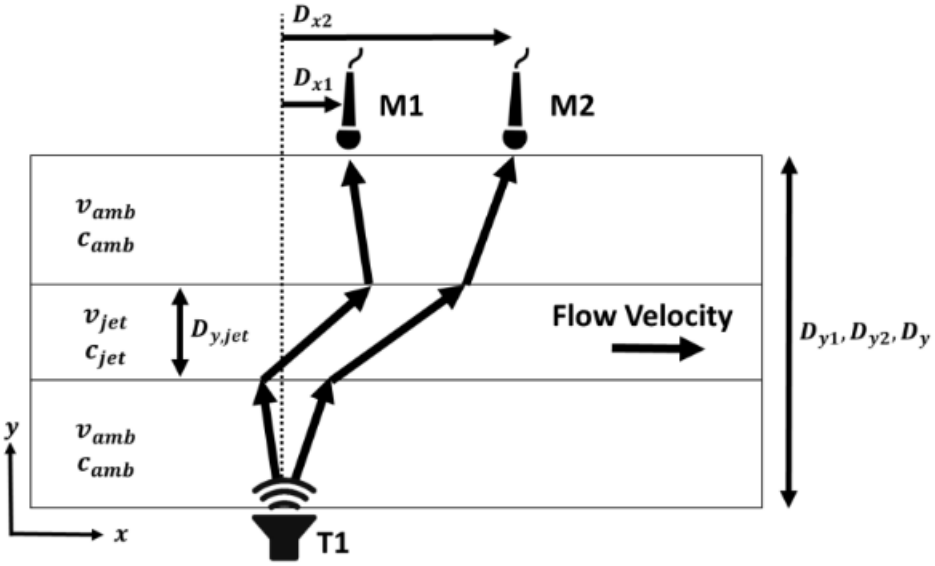

Figure 1: Application of Modified Sonic Anemometry in a non-uniform flow medium with known ambient conditions. Reproduced from Otero et al. [2]

DeSilva et al. [6] and Srinivasan et al. [11] explored sound source adequacy for TDE. These studies tended to focus primarily on the quality of the correlation result for each source, with concern regarding the SNR as opposed to overall SPL. In an environment as noisy as the exhaust flow of a jet engine, electronically driven sources are simply not loud enough. In [11], a single Hartmann generator driven at a sonic frequency (1.9 kHz) produced promising TDE results in an ambient environment. The Hartmann generator mechanism has the potential to have sufficient SPL, and has been adapted for operation the jet engine exhaust environment.

The dual Hartmann generator is an improved sound source developed for these measurements, consisting of a new arrangement of two closely spaced Hartmann generators. It was designed to be loud enough to be heard over the engine while being ultrasonic to avoid engine tones and mitigate personnel safety concerns. The purpose of using two Hartmann generators was to provide a modulation effect on the signal. The design has been detailed in **Appendix A,** and an exploration of the acoustic generation process of the new generator arrangement can be found in Lowe et al. [12].

B. Turbulent shear layers

When high temperature, high velocity exhaust flow exits from a jet engine core or bypass duct, interaction with the surrounding air results in the formation of a shear layer that grows as the jet propagates downstream. The size of the shear layer increases linearly, and consists of highly turbulent flow separate from the core jet flow.

One of the frequency-domain effects of these shear layers on acoustic waves have been studied and termed “haystacking”. Powles et al. [13] in particular has described and modeled the phenomenon. It is termed haystacking after the spreading transformation to the frequency spectrum of a tone as it passes through a jet, and is also known as spectral broadening. Powles et al. modeled an acoustic tone passing through a single shear layer, whereas in an actual bypass engine, there are

four shear layers to pass through (two bypass-ambient layers and two core-bypass layers (**Figure 2**)), with an expected enhancement of the haystacking effect, in addition to attenuation of the signal overall. An example of the resulting spectral transformation is shown in **Figure 3**. The majority of the original tonal content, as well as the broadened content, is decreased in amplitude, and mostly disappears below the level of the jet noise. This is not an unexpected effect given the overall thickness of the combined shear layers.

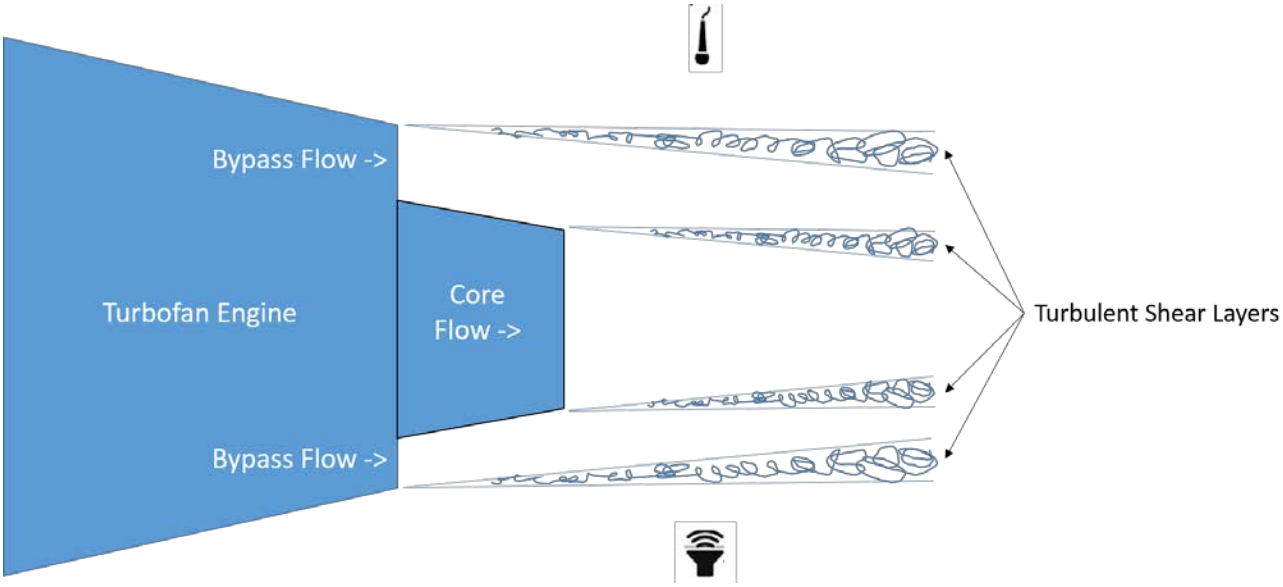

Figure 2: Bypass engine configuration, showing 4 tubulent shear layers. Two between the bypass flow and ambient, and two between the core and bypass flows

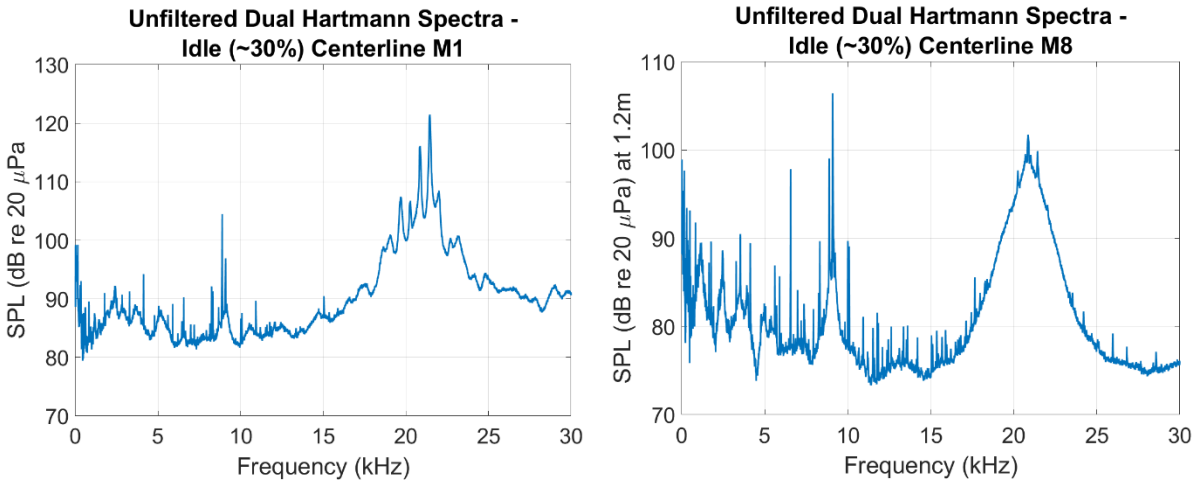

Figure 3: An example of haystacking as a signal is passed through bypass engine shear layers. As the approximately 20kHz tones pass through the shear layers, the signal is both attenuated and broadened, while retaining some tonal content. See [13] for a model of haystacking that approximates what is observed here.

Powles et al. note that "…in the high-frequency case, the process is essentially one of phase modulation: the sound propagates straight through the turbulence and undergoes a phase shift due to an effective fluctuation in the local refractive index." [13] Thus, for an ultrasonic signal, the data must be handled with care to mitigate the effects of haystacking. The choice of correlation method can drastically impact the accuracy of the time delay estimate. Haystacking as a phase and coherence affecting process must be taken into account.

C. Time Delay Estimation (TDE) Methods

The classic approach to estimating time delay between two signals has been the cross-correlation function,

$$R_{x_1,x_2}(\tau) = \int_{-\infty}^{+\infty} x_1(t)x_2(t+\tau)dt \tag{1}$$

where $x_{1,2}(t)$ are the signals to be correlated, τ is the lag, and $R_{x_1,x_2}(\tau)$ is the correlation function. With a spark source or similarly impulsive source, the signal in the frequency domain is broadband, and haystacking as a phenomenon has little impact on the lower frequency content, allowing for adequate cross-correlation.

When presented with the periodic signal of the Dual Hartmann in the jet noise environment, cross-correlation is not as reliable a method. The high frequency nature of the signal, along with phase randomness via the haystacking effect, may cause perturbations to $x_2(t+\tau)$ in the t-direction, thus causing $R_{x_1,x_2}(\tau)$ to not represent an accurate correlation, as x_1 and x_2 fail to align at the lagged value, τ. With a higher frequency signal, a minor perturbation in phase has a greater relative impact.

A more advanced approach is the generalized cross-correlation (GCC) of Knapp and Carter [9]. The GCC equation (Eq. 2) uses one of a number of processors (weighting functions) to filter the data according to the spectral content of the two signals:

$$R_{y_1,y_2}(\tau) = \int_{-\infty}^{+\infty} \psi(f)G_{x_1,x_2}(f)e^{i2\pi f\tau}df \tag{2}$$

where $G_{x_1,x_2}(f)$ is the Fourier Transform of the cross-correlation function, and is known as the cross-power spectral density (CPSD) of the two signals. $\psi(f) = H_1(f)H_2^*(f)$ is a processor that represents the combined effects of filters $H_1(f)$ and $H_2(f)$ applied to the signals. These filters H_1 and H_2 produce y_1 and y_2 when applied to x_1 and x_2, respectively. $R_{y_1,y_2}(\tau)$ is the *generalized* correlation function. If $\psi(f) = 1$, then $R_{x_1,x_2}(\tau) = R_{y_1,y_2}(\tau)$, and the standard cross-correlation (SCC) is recovered. Examining (2), it can be seen that the effects of haystacking on $\psi(f)G_{x_1,x_2}(f)$ will need to be minimized by choice of $\psi(f)$.

Knapp and Carter [9] present and compare a number of processors for the GCC (**Table 1**). Some of the processors, such as the Smoothed Coherence Transform (SCOT) and the Phase Transform (PHAT) [14] were developed "ad hoc" based on how they tend to affect certain classes of data. The primary focus of [9] is the Maximum Likelihood (ML) processor, which achieves the Cramér-

Rao lower bound on variance. However, this is a lower bound in theory, and is not always achieved in practice. Depending on the data, other processors may perform better. Additionally, under certain conditions, the TDE can suffer from large estimation errors, or anomalies. As noted by Ianniello in [15], these can be viewed as errors that violate an assumption from the derivation of the variance formula. Anomalous estimates are events that increase rapidly in likelihood below a certain SNR. It is beyond the scope of this work to develop a model of the probability of anomalies in the context of this experimental set-up. It will be shown however, that under certain conditions, the threshold effect of these large estimation errors is apparently observed.

Table 1: Knapp and Carter [9] table of GCC Processors

Processor Name	Processor or weight, $\psi(f) = H_1(f)H_2^*(f)$
Cross-Correlation	1
Roth Impulse Response	$1/G_{x_1,x_2}(f)$
SCOT	$1/\sqrt{G_{x_1,x_1}(f)G_{x_2,x_2}(f)}$
PHAT	$1/\lvert G_{x_1,x_2}(f)\rvert$
Eckart	$G_{s_1,x_2}(f)/G_{x_1,x_2}(f)$
ML or HT	$\dfrac{\lvert\gamma_{12}(f)\rvert^2}{\lvert G_{x_1,x_2}(f)\rvert(1-\lvert\gamma_{12}(f)\rvert^2)}$
Wiener	$\lvert\gamma_{12}(f)\rvert^2$

Phase Transform (PHAT)

The PHAT has a number of characteristics that make it attractive as a processor. It does not suffer from the same spreading that other processors do if there is uncorrelated noise [14]. It tends to suppress very strong tones, such as those produced by the engine. The dual Hartmann generator tends to produce tones that are broadened more than the jet tones due to the haystacking effect; so, this contributes to the relative success of this processor, as the processor includes more of the input from these broadened frequency bands.

Knapp and Carter focus on the ML processor, as they show that it minimizes variance to a value arbitrarily close to the Cramér-Rao Lower Bound (CRLB). However, Scarbrough [16] emphasizes that the CRLB is difficult to achieve in practice, as it requires an unknown "sufficiently long" sampling length. Scarbrough shows that each of the processors performs similarly at low SNR for his chosen simulated signal, and via experimentation and by applying some knowledge of the signal, the best processor can be identified. This approach was followed to confirm the superiority of the PHAT processor on the data from the present experiment.

3. Equipment and Experimental Procedure

Dual Hartmann generator and its signal

The dual Hartmann generator is a new acoustic signal generator that positions two small supersonic nozzles opposite two shallow cavities to set up an ultrasonic resonance. The signal emitted is a loud, two-tone ultrasonic continuous signal. based on two instances of the Hartmann resonance mechanism. Detailed descriptions of the dual Hartmann generator design are given in **Appendix A** and in Lowe et al. [12].

The use of the ultrasonic regime presents a new challenge as narrowband sources have a $2\pi/\omega$ time difference between peaks in correlation, making peak-finding in the correlation function a challenge for high values of ω $(= 2\pi f)$. This "2 pi ambiguity" is well-known, with a discussion of the issue given in [17, Introduction]. A modulation mechanism was needed to account for this, to allow for only one correlation peak in a time window corresponding to physically expected values. Placing two Hartmann generators in one package allows for two different ultrasonic tones, approximately 600 Hz apart, creating a "beat" frequency, f_b, and hence a modulation of the signal envelope. A sample time series of the signal is shown in **Figure 4**.

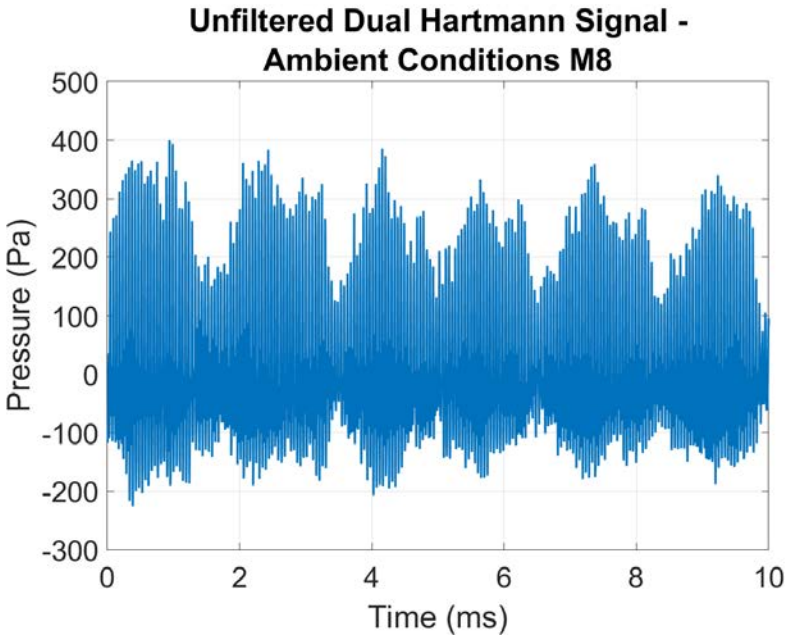

Figure 4: Sample of beat frequency produced by the dual Hartmann generator. Recorded in ambient air, 1.2m from source.

Figure 5 shows a labeled CAD drawing of the design. The resonance cavities used have slightly different depths to obtain the two different frequencies. Care was taken to avoid jet coupling (see Seiner et al. [18]) by spacing the nozzle-resonator pairs a reasonable distance (4 nozzle diameters center to center) apart within the chamber. The acoustic waves are emitted out of the chamber and through a small horn. The main body of the dual Hartmann generator is approximately 6"x6"x2", including the horn and the full air intake plumbing portions.

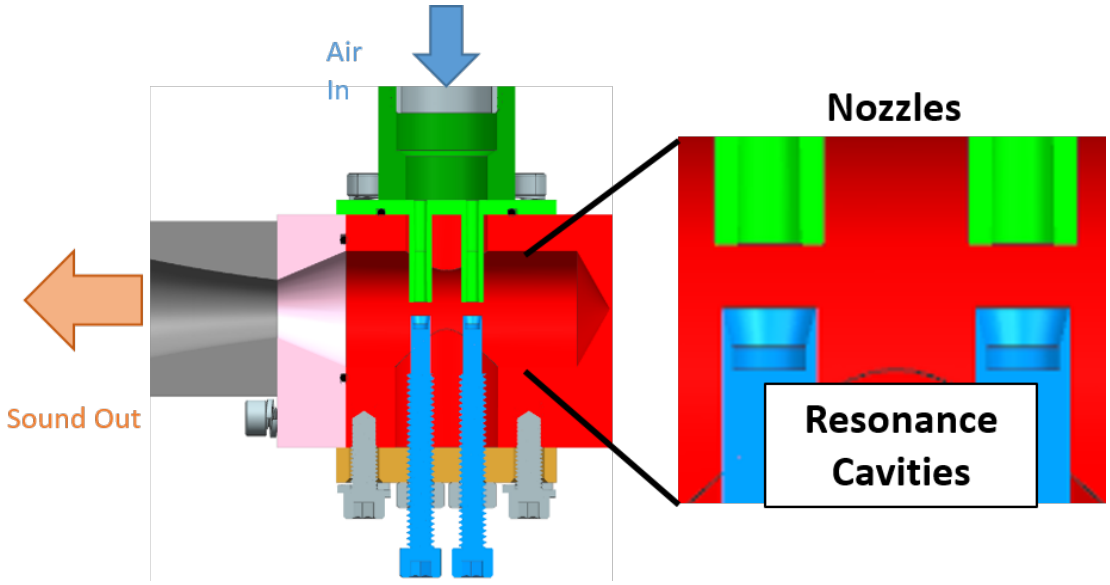

Figure 5: Dual Hartmann generator, complete with secondary chamber and horn attachment, and detail view of the supersonic nozzles and resonance tubes.

Benchtop experiments found the ideal nozzle-resonator spacing to provide for the dual-tone operation. In ambient conditions during the TFE731-2 experiment, the primary frequencies are f_1 = 20.9 kHz and f_2 = 21.5 kHz for a beat frequency $f_b = (f_2 - f_1)$ of ~600 Hz. **Figure 6** shows a representative spectrum.

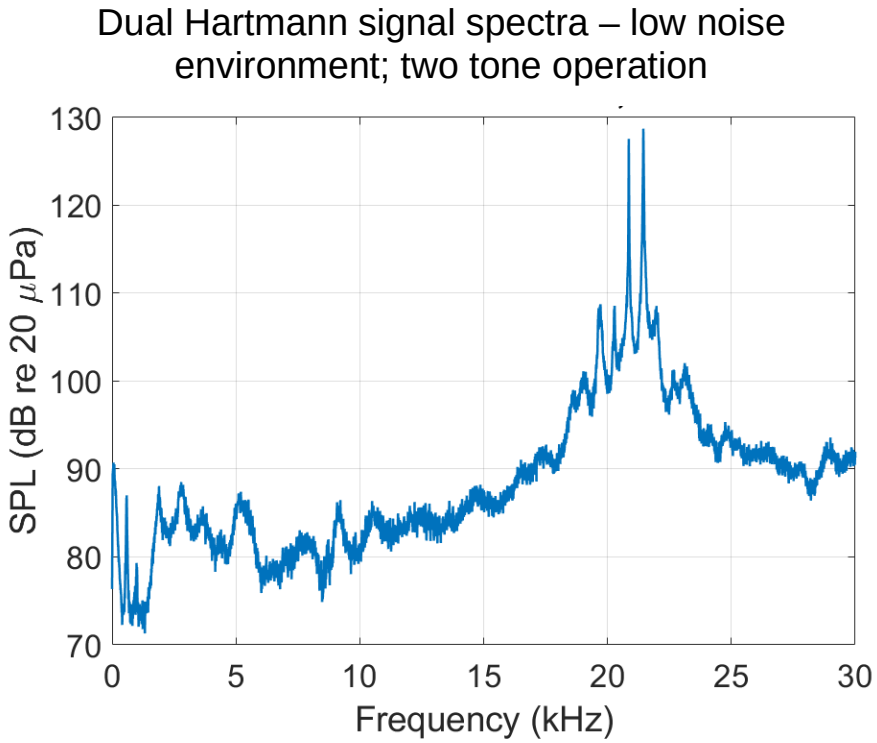

Figure 6: Dual Hartmann spectra displaying ambient condition two-tone signal. The primary tonal frequencies are f_1 = 20.9 kHz and f_2 = 21.5 kHz.

Engine Test

Testing was conducted on a Honeywell TFE731 turbofan research engine housed at the Turbomachinery and Propulsion Research Laboratory (Turbolab) at Virginia Tech. A microphone array consisting of ten PCB 378C10 pre-amplified microphones was positioned around the exhaust path of the engine. This is diagrammed in **Figure 7** (side view) and **Figure 8** (top view). A reference microphone (M1) was placed adjacent to the dual Hartmann generator to record a reference signal, while M2-M10 of the microphone array recorded the signal across the jet at various positions.

The equipment was placed such that the dual Hartmann generator was located 0.75 L/D_e downstream from the exhaust nozzle. This location was chosen to minimize the size of the shear layers encountered by the acoustic signal while ensuring no acoustic reflections off the nozzle itself.

The primary piece of equipment used to collect the microphone data was a PC-based NI Data Acquisition System. A PXIe-6358 card in a PXIe-1078 chassis collected the signals from two BNC-2110 terminal blocks. Between the microphone cables and the terminal blocks were a series of PCB 482C05 signal conditioners.

Tested conditions were based on the N_1 turbine corrected fan speed, N_{1Corr}, as a percentage of maximum speed. The operation points included 30% (also referred to as “engine idle” or “idle”), and 50% to 80% in 10% increments. Measurements were also taken at ambient, nominally quiet, conditions as a point of reference. N_{1Corr} is given by equation 3. T is the total inlet temperature.

$$N_{1Corr} = N_1/\sqrt{T/288.15\ K} \tag{3}$$

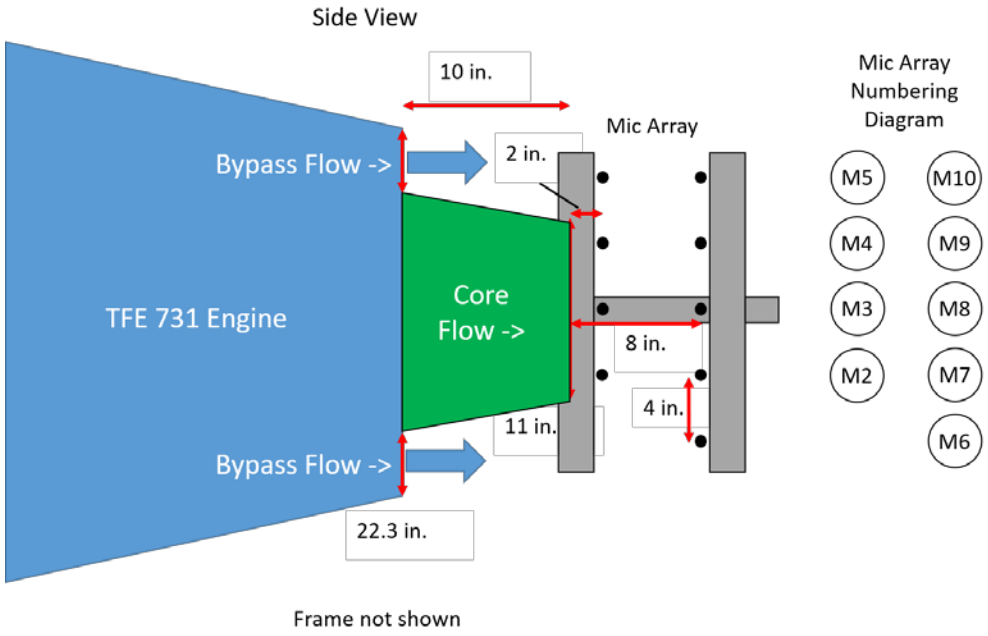

Figure 7: Microphone array placement relative to the TFE731 (side view). Dual Hartmann generator and Microphone 1 (M1) were at the same vertical position as M3 and M8, at the engine centerline.

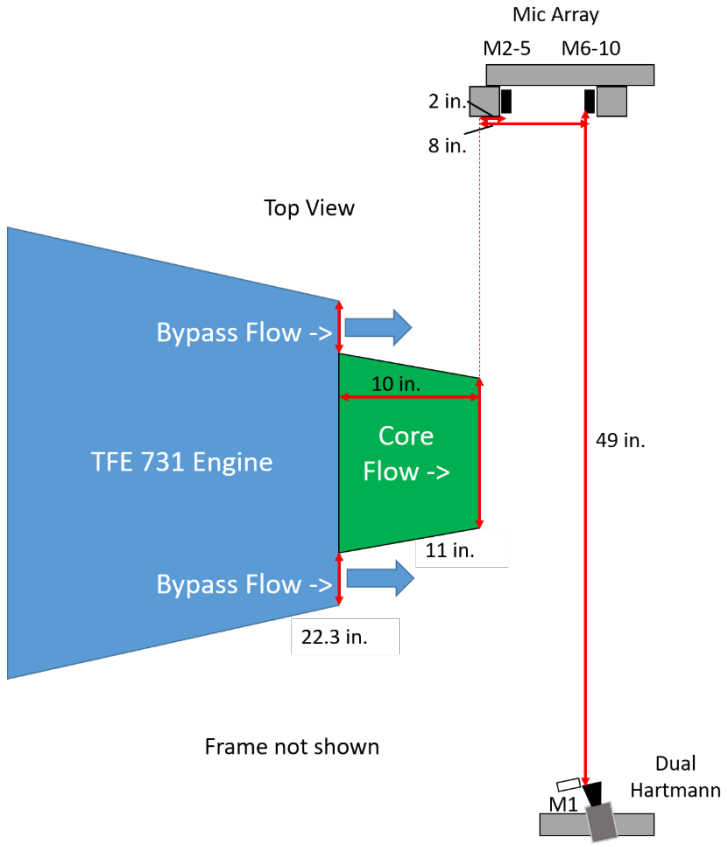

Figure 8: Microphone array placement relative to the TFE731 (top view).

Figure 9 is an annotated photograph of the test apparatus prior to final positioning aft of the engine. The dual Hartmann design is detailed in **Appendix A**.

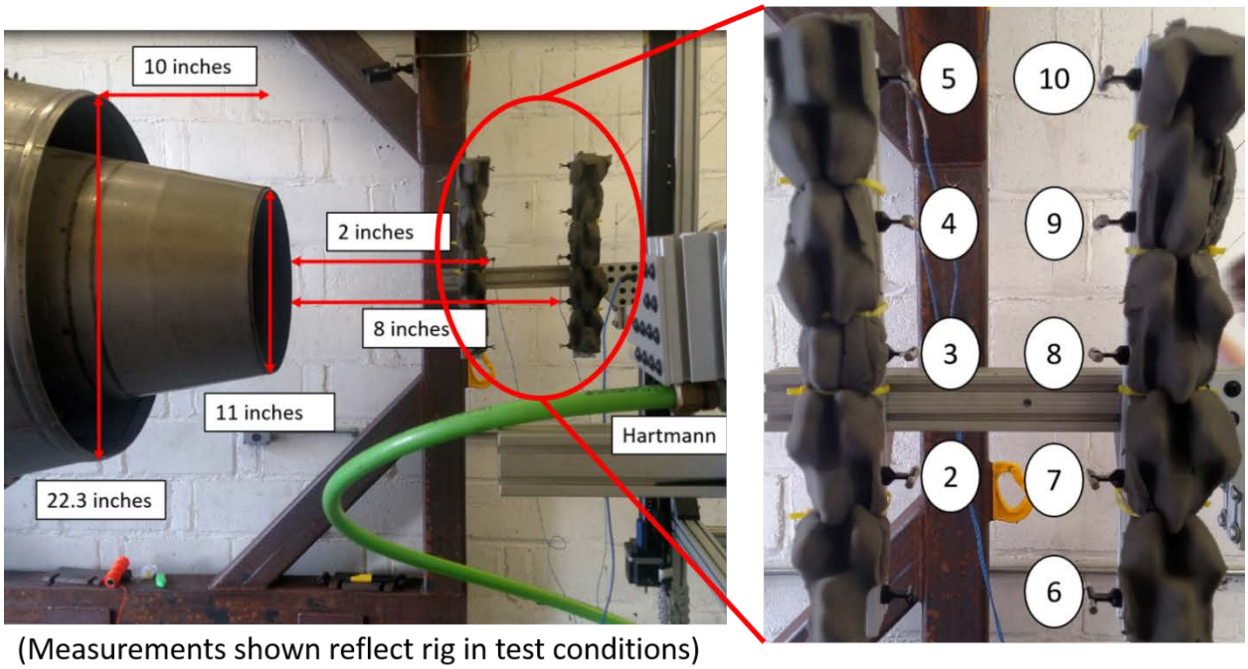

Figure 9: TFE731 Engine and Acoustic Measurement Rig

4. Data Processing Procedure

In order to estimate the time delay between recorded signals, the GCC approach [9] was followed. A comparison study between the various processor functions is shown here that demonstrates the superiority of the PHAT processor for use with this data.

GCC Processor Comparison

Initial investigations into various TDE methods found that the family of GCC processors, in particular the ML and PHAT processors, reduced the incidence of anomalous estimates the most overall. The comparison of processors is discussed in Section 2C. Other approaches, such as least-mean-square adaptive filtering [24] and bispectrum methods [25] were investigated, but failed to produce adequate results due to the nature of the jet noise.

Zhang and Abdulla [26] present a comparative study that discusses a wide range of TDE methods, including several that were not implemented on TFE731 engine data. The study looks at both a simulated dataset as well as actual noise. Primarily, this study compares three GCC processor methods (standard cross-correlation (SCC), Phase Transform (PHAT), and Maximum Likelihood (ML)) along with the average square difference function (ASDF) method. The ASDF method finds the squared difference between signals as a function of time delay τ, and thus requires no

computation in the spectral domain. Zhang and Abdulla found this to work best in a simulated domain, but with real data, PHAT performed best as SNR decreased [26, Section 5].

Appendix B contains additional details on the TDE approaches mentioned.

Data processing scripts were implemented that could easily swap GCC processors while keeping all other parameters equal so results could be compared. **Figure 10** shows the correlation results for several processors at engine idle, which best illustrates the difference in variance between the processor functions.

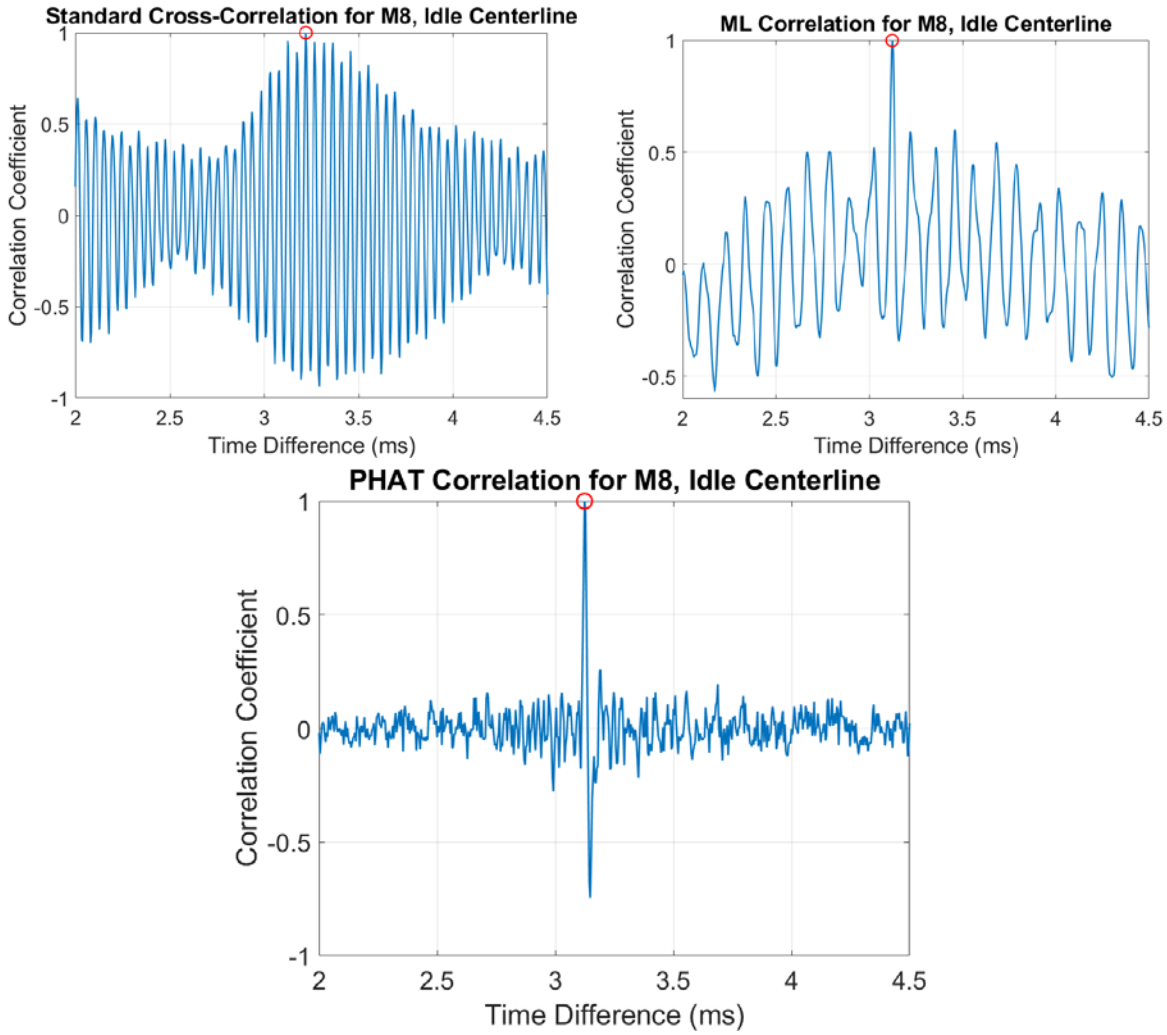

Figure 10: Three correlation functions (Standard (SCC), Maximum Likelihood (ML), and Phase Transform (PHAT) at the engine idle condition.

The Standard Cross-Correlation (SCC) appears as expected for a modulated high frequency signal, complete with evidence of the beat shape. With high SNR, the peak of this correlation produces good results, but the SNR even at the idle condition is too poor for there to be any confidence in this processor. The ML correlation produces a good estimate of TOF at the idle condition, but with already present evidence of potentially anomalous peaks. The ML processor is similar to the PHAT, but with additional weighting by the magnitude-squared coherence. Due to the haystacking

phenomenon, signal coherence across the jet is relatively poor. Introducing this additional weighting thus increases the propensity that errant spectral content, such as lower frequency jet noise, influences the correlation results. At engine idle, this is evident by the significant number of correlation peaks above 0.5 correlation coefficient. These anomalies increase at higher engine conditions with this processor. By removing this coherence weighting factor, we return to the PHAT:

$$\psi(f) = \frac{1}{|G_{x_1,x_2}(f)|} \tag{3}$$

As discussed in Section IIC, with uncorrelated noise (i.e., $G_{n_1,n_2}(f) = 0$), this would produce a Dirac δ function at the exact time delay, whereas other processors will experience some spreading [9]. This is close to the result seen in the PHAT correlation of **Figure 10**.

Appendix C contains additional comparisons of datasets between the PHAT, ML, and SCC correlations at engine conditions beyond idle. These illustrate that the ML correlation is influenced less by the (low) coherence of the signal and more by the (moderate) coherence of lower frequency jet noise.

In order to estimate time delays, each of the far-field microphones, M2-M10, were correlated with the reference microphone M1. Filtering the data was found to be unnecessary, as the GCC is effectively an automatic filter on the data. To form the processor $\psi(f)$, an estimate of the cross-power spectral density (CPSD), $\hat{G}_{x_1,x_2}(f)$, is needed. It was generated with the cpsd() function in MATLAB for each of the samples. Segment lengths of 50,000 samples and a 50% overlap were used, with a Hanning window applied. Each of these estimates were averaged over all of the samples to then form $\hat{\psi}(f)$ as used in Equation (4).

$$R_{y_1,y_2}(\tau) = \int_{-\infty}^{+\infty} \hat{\psi}(f) G_{x_1,x_2}(f) e^{i2\pi f\tau} df = \int_{-\infty}^{+\infty} \frac{1}{|\hat{G}_{x_1,x_2}(f)|} G_{x_1,x_2}(f) e^{i2\pi f\tau} df \tag{4}$$

Each sample was then weighted and a correlation function, $R_{y_1,y_2}(\tau)_n$, produced. These were then averaged to produce an average correlation function for that microphone pair. The maximum in the interval was found to be the estimate of time delay.

The full set of codes are available in **Appendix E**.

5. Results and Discussion

The conditions tested will be referred to by the N1 Corrected Fan Speed (N_{1Corr}) as a percentage of maximum. Ambient refers to the engine-off condition, and engine idle is roughly 30%. Other conditions tested include 50%, 60%, 70%, and 80%. Each increase in N_{1Corr} represents an increase in engine power, thrust, average exhaust velocity, and average exhaust temperature. Correspondingly, noise levels produced by the jet are louder, and the turbulence environment with the shear layers is more intense. The M1 and M8 data are used as typical of the reference and across-jet signals to illustrate the data processing sequence.

A. Time-Domain Signal Samples

Samples of the raw signal over 10 ms at ambient condition are shown in **Figures 11** and **12**. **Figure 11** is from the reference microphone adjacent to the dual Hartmann horn exit, while **Figure 12** is at M8, 1.2 m away. The beat frequency shows up as the envelope of the signal.

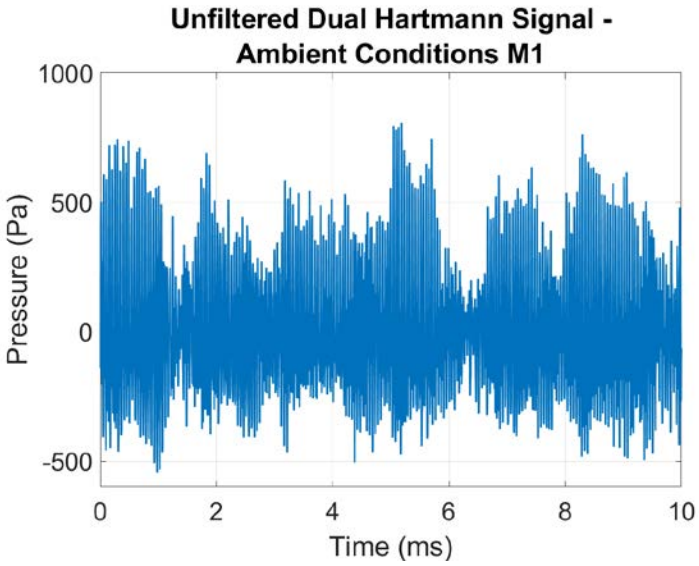

Figure 11: Raw signal in ambient at M1

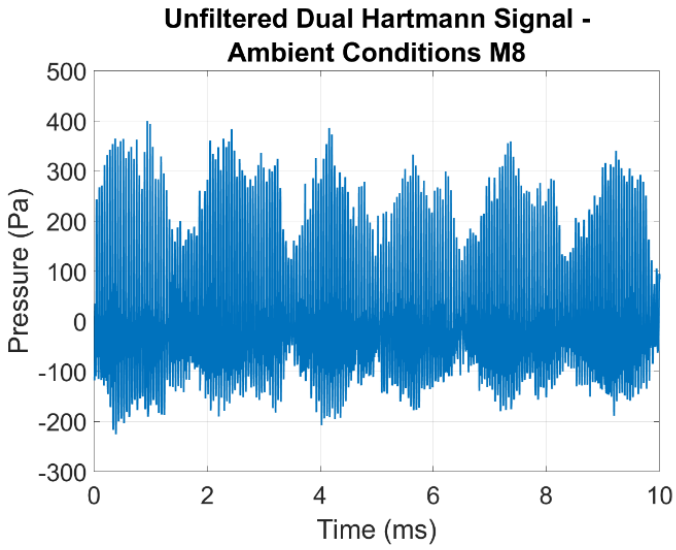

Figure 12: Raw signal in ambient at M8. Scale differs from **Figure 11** due to source/receiver distance.

The raw signal at M8 is shown in **Figures 13** and **14** at engine idle and 80%. At the idle condition, the beat structure is roughly identifiable, while at the 80% condition it is indiscernible.

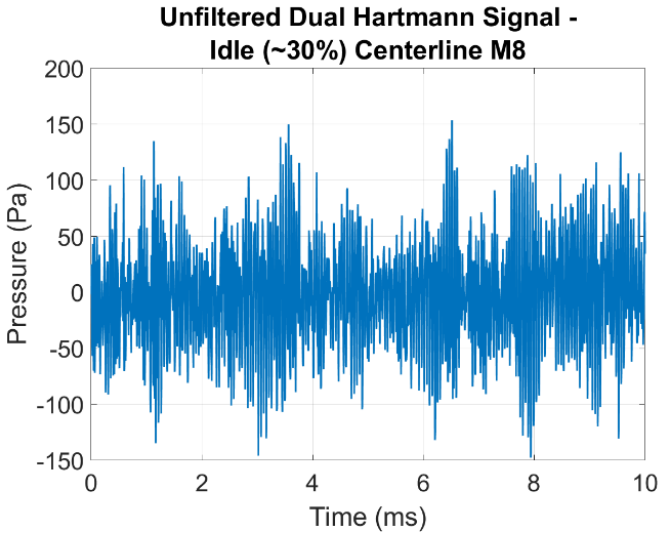

Figure 13: Raw signal at M8 at engine idle

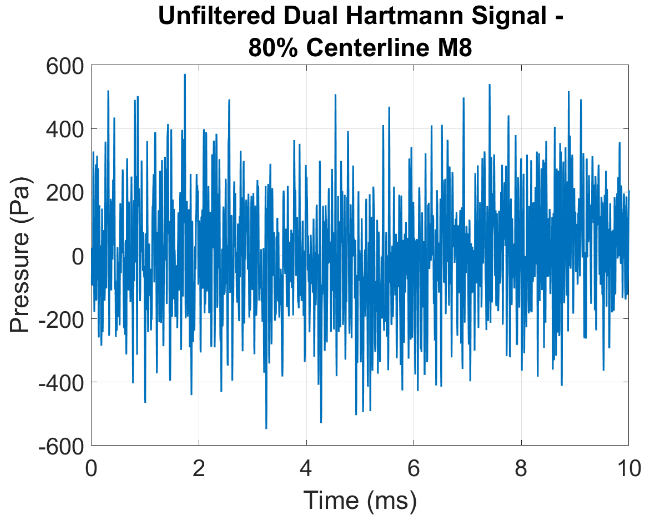

Figure 14: Raw signal at M8 at N_{1Corr} = 80%. As engine speed increases, the magnitude of the peak-to-peak signal increases due to increased engine noise.

B. Spectra

Figures 15 and **16** show spectral estimates of the signal at ambient and at an extreme condition, N_{1Corr} = 70%. The N_{1Corr} = 80% spectra suffers from intense spectral broadening, to the extent that the Hartmann generator signal can not be reliably discerned. The ambient spectrum shows two dominant peaks at the fundamental frequencies, with the f_1 tone being 10 dB higher than f_2. When the engine is on, this dominance is apparent as the center-point for the spectral broadening phenomenon. This relative dominance of f_1, along with the spectral broadening effect overall, is thought to contribute to the degrading quality of the correlations. The sound level of f_1 is above the noise levels all the way up to N_{1Corr} = 70%, leading to one area of possible improvement: ensuring the f_2 tone is raised to the level of the f_1 tone. The tuning process for the Hartmann generator results in small differences in signal generation quality. Optimizing this process would result in equal strength tones.

The spectrum with the engine on also shows dominant engine tones not from the dual Hartmann. The microphones are very near the exhaust plane, and the presence of strong jet tones and harmonics is to be expected. The PHAT processor effectively filters out the influence of these extremely narrow tones.

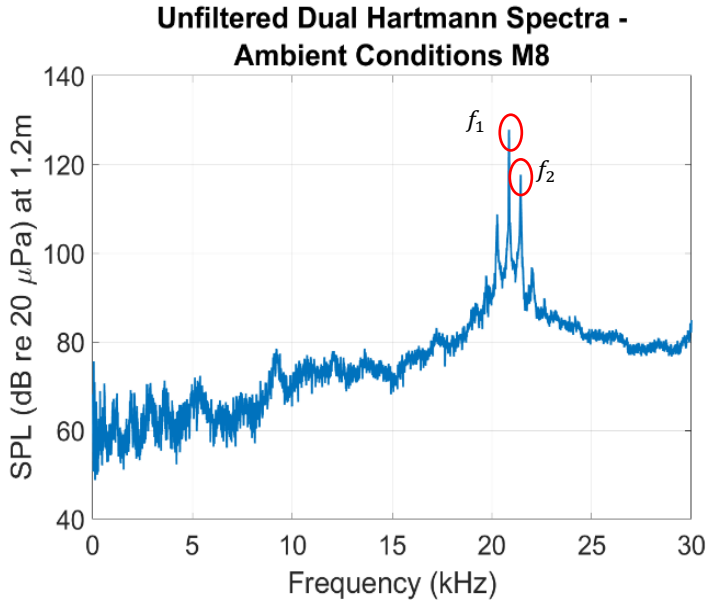

Figure 15: Spectrum of the received signal at M8 in ambient conditions

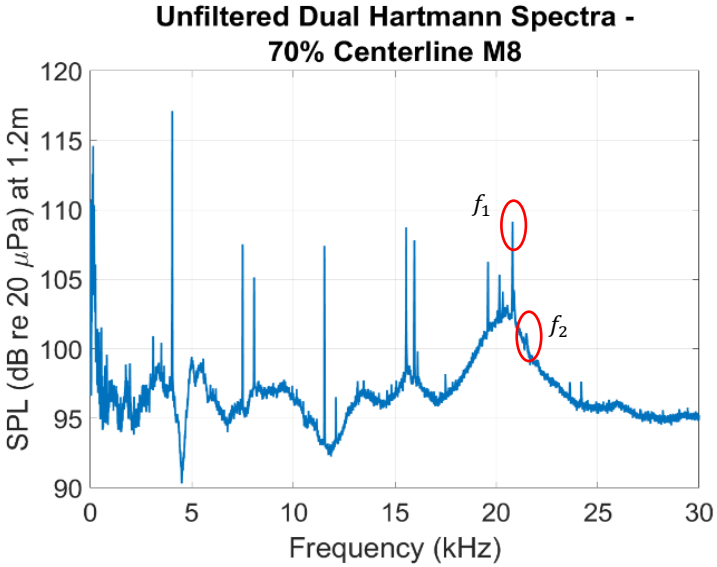

Figure 16: Spectrum of the received signal at M8 at N_{1Corr} = 70%

C. PHAT Correlation Figures

PHAT correlation functions from this test show how increasing noise levels and turbulence-caused haystacking increase the variance. As Scarbrough [16] points out, variance for correlators can be thought of as a combined effect of the probability that (a) there is a nearby anomalous peak that is incorrectly chosen as the time delay and (b) the correct peak is chosen, but it varies from the true time delay by some amount. Except in the ambient condition where the correlators agree, there is no a priori knowledge of the precise time delay. As such, the presence of anomalous peaks will be the prime criterion in determining whether the correlator is reliable at that condition.

Figures 17 highlight the PHAT correlation functions between M1 and M8, presented in order of increasing engine thrust. With increasing engine thrust comes a noisier flow medium and higher haystacking intensity. These contribute to an increase in variance on the PHAT correlations.

The PHAT correlations at the lower engine conditions (ambient, engine idle, and N_{1Corr} = 50%) resemble a δ function or impulse at a single τ. At higher engine conditions (N_{1Corr} = 60%+), anomalous peaks are present with higher correlation coefficients, and there is less confidence in the estimate. For the microphone, M8, shown in **Figures 17**, the N_{1Corr} = 70% correlation appears to have fewer anomalous peaks than the N_{1Corr} = 60% correlation, but this is not always the case. The ability of the PHAT correlation to produce reliable TOF estimates hits a definitive limit between N_{1Corr} = 70% and 80%. The threshold effect described by Ianniello [15, Figure 4] is being observed in the vicinity of N_{1Corr} = 70%, and even at N_{1Corr} = 60%. At the N_{1Corr} = 80% condition, anomalous peaks are persistent throughout the time window. Here, the jet noise, shear layer environment, and resulting spectral broadening is too extreme, resulting in a variance in the correlation that is too high for reliable TDE.

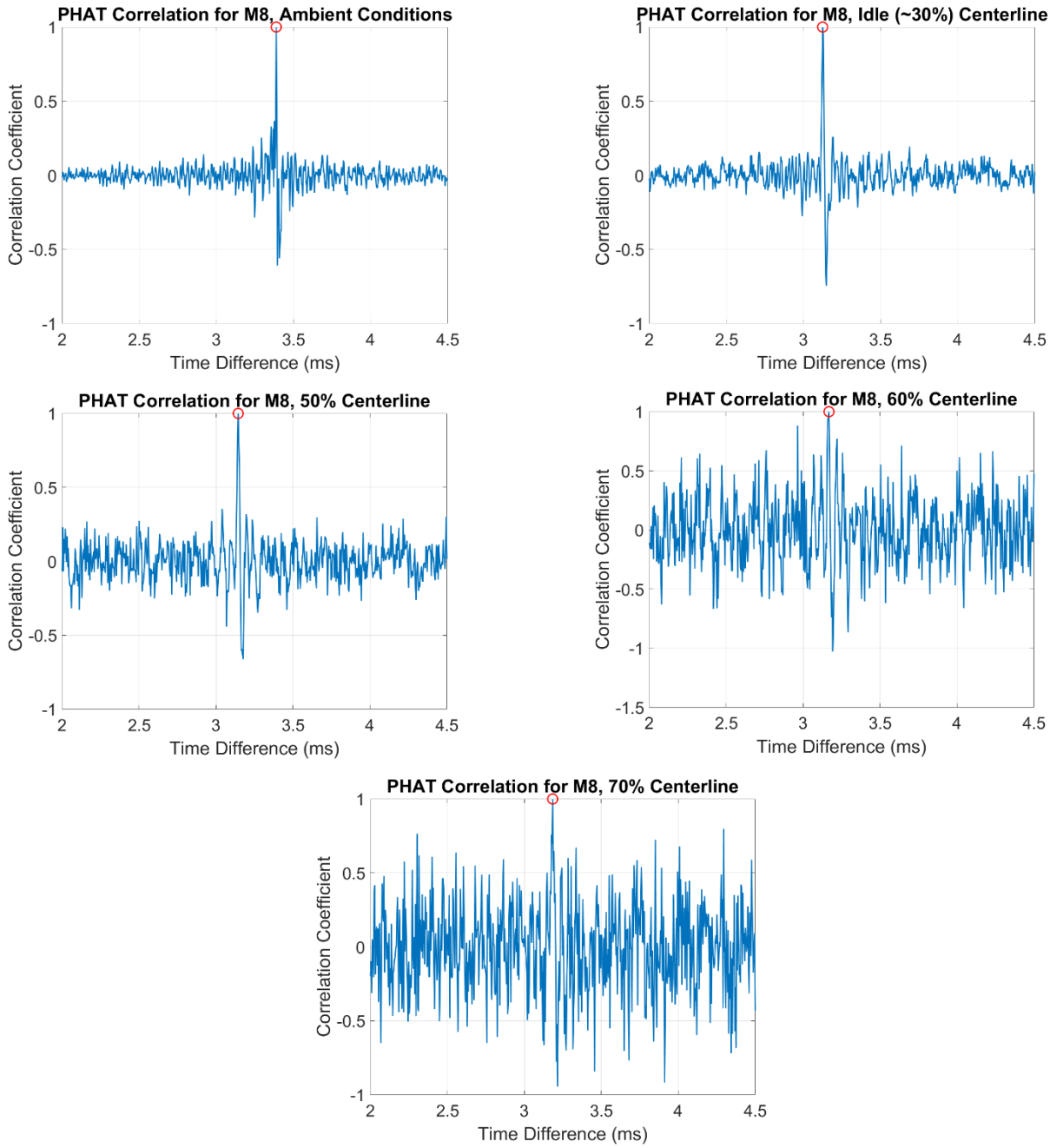

Figures 17: PHAT Correlations at M8 for engine conditions (N_{1Corr}) from Ambient to 70%.

At $N_{1Corr} \leq 70\%$, improved confidence in the TDE for individual microphones can be obtained by plotting peaks from the entire array of microphones and comparing to expected patterns. **Figure 18** shows the peak of the correlation function versus microphone number. Delays in the reduced window of 3-3.5 ms are shown to highlight the differences between conditions. The expected trend, for a given condition, is a shallow 'U' shaped bowl of time delays in each plane. This is demonstrated in **Appendix D** for the ambient condition. This is seen intuitively based on M1-M#

relative distances as seen in **Figures 7** and **8**. M3 and M8 are expected to have the shortest time delay. The upstream plane (M2-M5) will have longer time delays than the downstream plane (M6-M10) in ambient, although the inter-plane TOF difference will vary depending on the flow conditions due to the shortest integrated acoustic ray path varying strongly with flow velocity. Future work may involve using the microphone relationships to create a peak-finding "gate", similar to that described in Ianniello [15], wherein *a priori* information is used to aid in accurate peak-finding.

As the average temperature of the jet is higher than the ambient temperature, the reduction in TDE for all non-ambient conditions is expected. An increase in TDE as the engine speed is increased is expected as increasing jet velocity results in longer acoustic ray paths.

Figure 18 also makes clear that the upstream plane results form a more consistent pattern. This is attributed to clearer received signals in the upstream propagation, which matches early qualitative models. In contrast, the downstream signals suffer from anomalous selections at several points, particularly M7 at N_{1Corr} = 60% and 70% and M10 at N_{1Corr} = 60% (off the chart). Future work may entail re-designing the geometric arrangement of the microphone array relative to the jet, being sure to not negatively affect the ability to perform tomography.

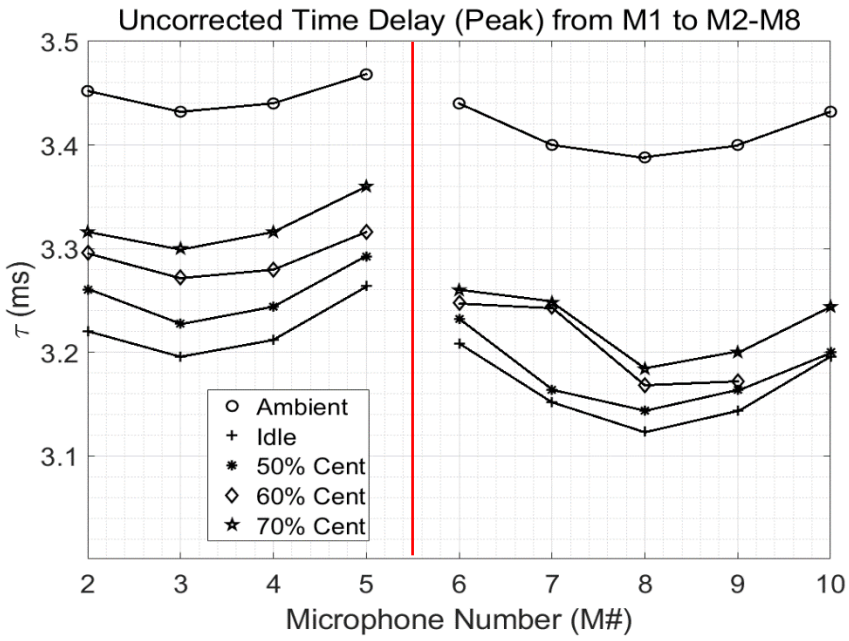

Figure 18: PHAT Correlation TDE results for the entire microphone array. The vertical lines separate the two planes of microphones (see **Figures 7**, **8**).

Based on the pattern-finding guidelines discussed in this section, a reasonable lower bound for the percentage of anomalous selections for each condition is as follows - ambient and idle: 0%; N_{1Corr} = 50%: 11% (1, M10); N_{1Corr} = 60%: 33% (3, M7, M9, M10); N_{1Corr} = 70%: 11% (1, M7).

6. Conclusions and Future Work

Jet engine exhaust flow is one of the most challenging flow environments for performing TDE, considering not only the very high baseline noise level but also the turbulent shear layer effects on the signal. Presented here is a new signal and signal generator that show promise in overcoming those challenges and a data processing technique study that improves on the standard cross-correlation approach.

The dual Hartmann generator is an attractive concept for its packaging and signal properties, with high sound level ultrasonic operation. Potential improvements to the design include louder overall tones and achieving a lower sound level difference between the tones f_1 and f_2. Future prototypes are capable of fitting into an even smaller packaging arrangement, considering the fundamental nozzle-resonator assembly is quite compact.

The PHAT processor serves to tackle the challenge of the haystacking effect by taking into account the full range of content from the broadened tone. For a given signal and flow regime, a study can be rapidly performed to determine if PHAT or another processor produces the best result. At N_{1Corr} = 80%, neither the PHAT processor nor any other GCC processor produced an unambiguous result that can be used for reliable measurements.

An upper limit for this pairing of engine and sound source has been identified which leaves room for a range of (a) lower noise applications and (b) dual Hartmann generator improvement directions. Potential lower noise applications for the current dual Hartmann generator include smaller engines and inlet duct mass flow measurements. Dual Hartmann generator potential improvements include an overall increase of SPL and equalizing the difference between the tones f_1 and f_2. Further reductions in packaging without sacrificing SPL are another area for design exploration. If these improvements can be made, the attractive design features of the dual Hartmann generator can be retained. These include (a) ultrasonic operation, (b) relatively compact packaging, (c) no moving parts, and (d) no electronic components.

In the case of improvements to the dual Hartmann generator acoustic output, the upper limit on both engine exhaust diameter and engine speed should increase.

References

[1] K. Daniel et al., “Experimental Investigation of the Pressure Field of a Heated Supersonic Jet with a Centered Total Temperature Non-Uniformity”, AIAA Aviation Forum, 2018, DOI: 10.2514/6.2018-3145

[2] R. Otero Jr., K. T. Lowe, and W. Ng, “Extension of sonic anemometry to high subsonic Mach number flows”, Measurement Science and Technology, 28(3), 2017, DOI:10.1088/1361-6501/aa54ed

[3] R. Otero Jr., K. T. Lowe, and W. Ng, “Non-Intrusive Acoustic Measurement of Flow Velocity and Temperature in a High Subsonic Mach Number Jet”, Measurement Science and Technology, 29(1), 2017, DOI:10.1088/1361-6501/aa92a9

[4] R. Otero Jr., K. T. Lowe, W. Ng, K. Silas, “Coupled Velocity and Temperature Acoustic Tomography in High Subsonic Mach Number Flows”, Measurement Science and Technology, 30(10), 2019

[5] R. Otero Jr., K. T. Lowe, W. Ng, L. Ma, C. Kim, “Non-Intrusive Gas Turbine Engine Exhaust Characterization using Acoustic Measurement”, AIAA J. Propulsion and Power, 34(3), p. 730-738, 2017.

[6] U. DeSilva, R. H. Bunce, J. M. Schmitt, and H. Claussen, "Gas Turbine Exhaust Temperature Measurement Approach Using Time-Frequency Controlled Sources", in *Proceedings of ASME Turbo Expo 2015*, 2015.

[7] D. Wilson and D. Thomson, “Acoustic Tomographic Monitoring of the Atmospheric Surface Layer”, J. of Atmospheric and Oceanic Technology, Vol. 11, 1994, p. 752

[8] J. Hartmann, and B. Trolle, “A new acoustic generator. The air-jet generator”, J. Sci. Instrum. 4, 1927, p. 101.

[9] C. Knapp, and G. Carter, “The Generalized Correlation Method for Estimation of Time Delay”, IEEE TRANS. ON ACOUSTICS, SPEECH, AND SIG. PROC., ASSP-24 No. 4, 1976, p. 320.

[10] E. Robinson and A. Quazi, “Effect of sound-speed profile on differential time-delay estimation”, The Journal of the Acoustical Society of America, 77 (3), 1086 (1985)

[11] K. Srinivasan et al., “Effects of acoustic source and filtering on time-of-flight measurements”, Applied Acoustics, 70, 2009, p. 1061-1072

[12] K. Lowe, K. Silas, G. Boggs, and W. Ng, “An experimental study on the coupling between adjacent Hartmann whistles”, Int’l J. of Aeroacoustics 18(2-3), 299-316, 2019

[13] C. Powles et al., “A weak-scattering model for turbine-tone haystacking outside the cone of silence”, International Journal of Aeroacoustics, Vol. 10, No. 1, 2011

[14] G. Carter et al., “The Smoothed Coherence Transform”, Proceedings of the IEEE, Vol. 61, No. 10, 1973, p. 1497

[15] J. Ianniello, "Time delay estimation via cross-correlation in the presence of large estimation errors," in *IEEE Transactions on Acoustics, Speech, and Signal Processing*, vol. 30, no. 6, pp. 998-1003, December 1982, doi: 10.1109/TASSP.1982.1163992.

[16] K. Scarbrough, “Analysis of Time Delay Estimator Performance”, NUSC Technical Report 7203, 1984

[17] E. Weinstein and A. Weiss, “Fundamental Limitations in Passive Time-Delay Estimation – Part II: Wide-Band Systems”, IEEE TRANS. ON ACOUSTICS, SPEECH, AND SIG. PROC., ASSP-32 No. 5, 1984, p. 1064.

[18] J. Seiner et al. “Dynamic Pressure Loads Associated with Twin Supersonic Plume Resonance”, AIAA Journal, Vol. 26, No. 8, 1988, p. 954

[19] G. Raman and K. Srinivasan, “The powered resonance tube: From Hartmann’s discovery to current active flow control applications”, Progress in Aerospace Sciences, 45, 2009, 97-123

[20] J. Kastner and M. Samimy, “Development and Characterization of Hartmann Tube Fluidic Actuators for High-Speed Flow Control”, AIAA Journal, Vol. 40, No. 10, October 2002

[21] S. Narayanan et al., “Aero-acoustic features of internal and external chamfered Hartmann whistles: A comparative study”, Journal of Sound and Vibration, 333 (2014), 774-787

[22] G. Raman et al., “Development of Powered Resonance-Tube Actuators for Aircraft Flow Control Applications”, Journal of Aircraft, Vol. 41, No. 6, Nov-Dec 2004

[23] E. Brun and R.M.G. Boucher, “Research on the Acoustic Air-Jet Generator: A New Development”, The Journal of the Acoustical Society of America, Vol. 29, No. 5, 1957

[24] S. Chern and S. Lin, “An adaptive time delay estimation with direct computation formula”, The Journal of the Acoustical Society of America, 96, 811 (1994)

[25] C. Nikias and R. Pan, “Time Delay Estimation in Unknown Gaussian Spatially Correlated Noise”, IEEE Trans. On Acoustics, Speech, and Signal Processing, Vol. 36, No. 11, Nov. 1988

[26] Y. Zhang and W. Abdulla, “A Comparative Study of Time-Delay Estimation Techniques Using Microphone Arrays”, University of Auckland School of Engineering Report No. 619

[27] G. Boggs, “Turbine Engine Thrust Measurements Using a Non-Intrusive Acoustic Technique”, Virginia Tech M.S. Thesis, 5/8/2019

Appendix A: Hartmann Generator Detailed Design

Motivation

The requirement for a next generation sound source was evident by the results of a previous engine experiment [5], which determined that the signal-to-noise ratio (SNR) of the existing spark source was insufficient at the most challenging engine condition. Internal research determined that electronically driven sources at the size required for a 'point source' assumption would not be loud enough. This led to a development effort of compressed air driven sound sources, including concepts such as air horns, Hartmann generators, also known as Hartmann whistles, and other whistle devices. In the research field of time delay estimation (TDE), there exist investigations of the adequacy of various sound source types (see [6] and [11]). The Hartmann mechanism was particularly promising for its relatively simple design, lack of moving parts, lack of electronic parts, high potential sound pressure level (SPL) (and thus SNR), and excellent performance in a quiescent environment relative to other methods [11].

Hartmann Mechanism Background

The Hartmann generator (Hartmann and Trolle [8]) concept employs a nozzle supplied with compressed air aimed to flow directly into a resonator cavity. This flow is then ejected from the cavity, which is then quickly refilled. This unsteady periodic motion is a high-frequency oscillation that manifests as a loud narrowband tone. The phenomenon has been studied extensively, such as by Lowe et al. [12] and as seen in a review on Hartmann generators by Raman and Srinivasan [19]. Depending on flow conditions and geometric parameters, one or more acoustic mechanisms present themselves to create the tonal noise. These are termed the jet instability mode, the jet screech mode, and the jet regurgitant mode [19, Table 3].

Various studies on the design space of Hartmann generators were used as the basis for several design choices. Work by Kastner and Samimy [20], Narayanan et al. [21], and Raman et al. [22] provided design guidance in terms of the geometric parameters of the Hartmann nozzles, resonator depth, diameter, chamfer, lip thickness, and nozzle-resonator offset distance. Brun and Boucher [23] describe a "secondary resonating chamber", which influenced an enclosing chamber for this design.

Signal Design

The desired signal for the sound source is either a pulsed signal, modulated signal, or low enough frequency signal in order to perform reliable correlations that make up the TDE process. With the Hartmann generator, pulsed operation is difficult due to challenges in rapidly starting and stopping the compressed air jet while enabling the generator to achieve steady signal output.

A large-sized generator is required for the Hartmann generator to achieve a low enough frequency for the purposes of engine exhaust TDE. The desired frequency, f, is less than around 500 Hz, as a higher frequency signal correlated with a lagged version of itself has correlation peaks at $\tau_k = \tau_0 \pm k/f$ for integer values of k. To ensure only one τ value appears in a given window of physically possible lags, f must be of sufficiently low value. At 500 Hz, a peak is expected to

appear every 2ms. The difference between the fastest signal transit time and the slowest across a representative large jet is approximately 1.33ms, resulting in an upper frequency limit of 750 Hz. Applying a 1.5x safety factor, 500 Hz became an upper limit design goal.

An approximate formula for the Hartmann operating frequency is given by Raman et al. [19, equation 4], and reproduced as equation A1:

$$\frac{\lambda}{4} = L_r + 0.3D_r \tag{A1}$$

, where λ is wavelength, L_r is the cavity length of the resonator, and D_r is the resonator diameter. The 0.3 D_r term represents a correction factor for end effects. This equation is known to suffer from inaccuracies due to non-linear effects, particularly for "short tubes".

For a 500 Hz frequency, this would result in a length of approximately 0.17m, or 7 in. In addition, nozzles, a compressed air supply, nozzle-resonator spacing, and additional hardware would add considerable overall length in the primary dimension. With future applications in mind, a sound source of this overall size is unacceptable. Furthermore, a source that operated primarily at 500 Hz has drawbacks in that it could cause equipment interference and/or interfere with the safety of personnel.

The last type of signal is a modulated one, which can be achieved by producing a pair of closely spaced tones with a frequency difference of approximately 500 Hz or less. This creates a beat frequency, a simulation of which is shown in **Figure A1**. With this, ultrasonic tones (>20kHz) can be used. For example, 22.0 kHz and 24.0 kHz are used in the simulated example.

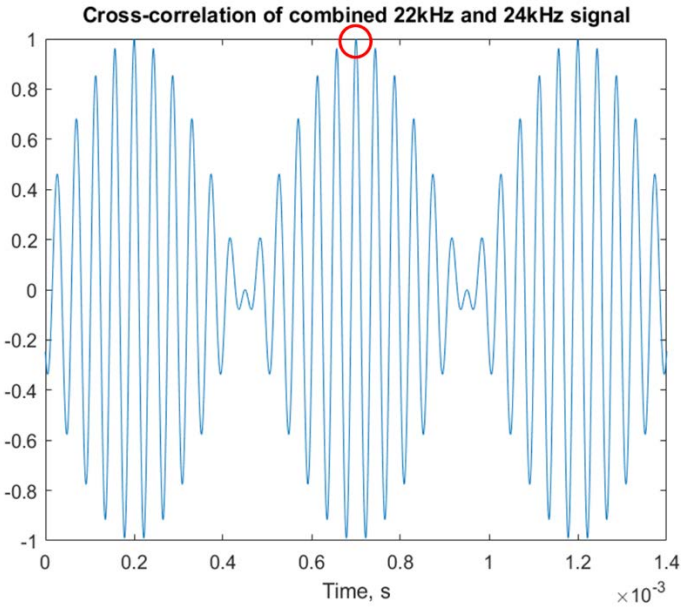

Figure A1: Simulated cross-correlation of a two-tone signal. Developed prior to implementation of generalized cross-correlation approach.

Operating in the ultrasonic range has numerous advantages, including: (a) mitigating concerns over equipment interference; (b) mitigating concerns over personnel sound exposure, as Occupational Safety and Health Administration (OSHA) limits on noise exposure are higher for ultrasonic sources; (c) reduced risk of interference with sonic jet tones that vary with engine parameters and may not be known a priori; and (d) a design advantage allowing for a compact package for Hartmann resonators, as the resonator length is on the order of 3mm, instead of 170mm.

Overall Package

The packaging of the resonators was driven by research by Brun and Boucher [23, p. 580] claiming an increase in acoustic power produced by incorporating a "secondary" resonating chamber. The nozzle and resonators are enclosed in a chamber through which excess air coming from the nozzles passes through an exhaust port and the acoustic waves are focused through a side port. A further acoustic emissions enhancement is achievable with the addition of a horn at the acoustic exit.

The dual Hartmann design was based on a design concept from the NASA Langley Research Center, as shown in **Figure A2**. This concept was scaled down in an approximate way, while swapping out a single nozzle-resonator for a dual nozzle-resonator assembly. (Credit to Martha Brown, Research Engineer, for providing these images).

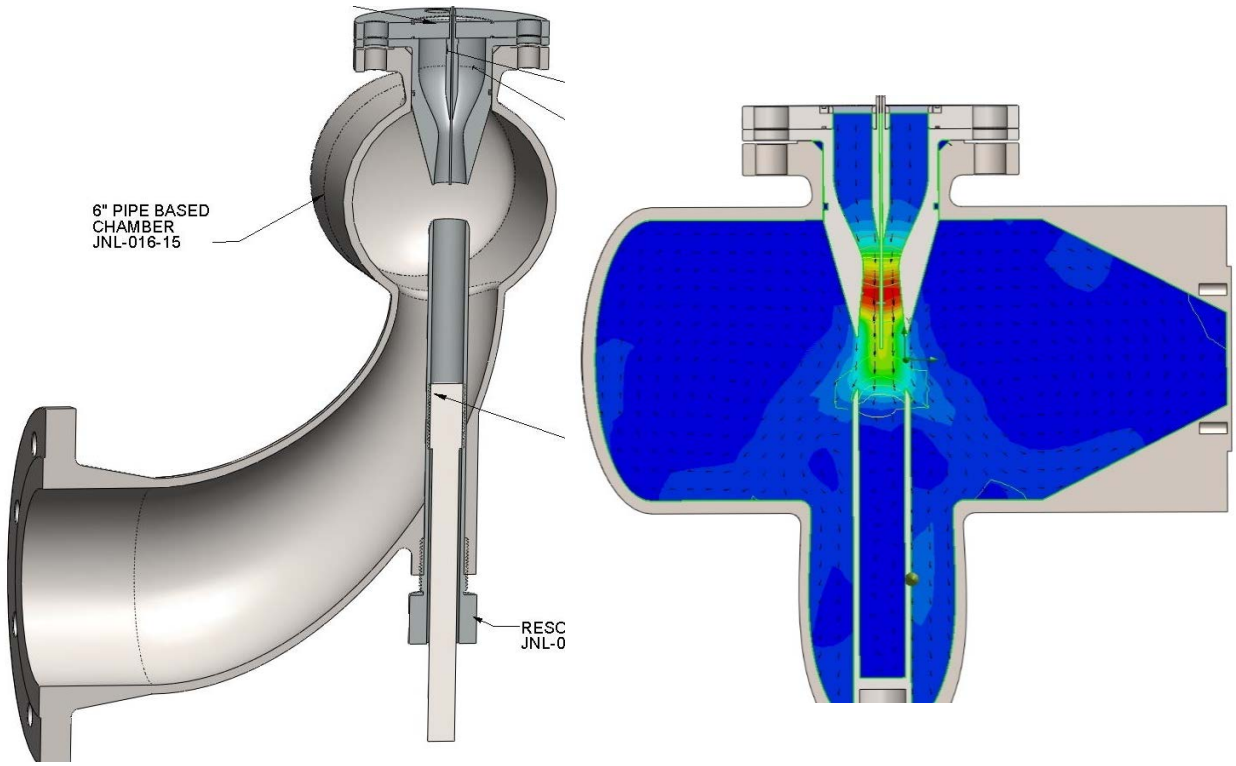

Figure A2: NASA Langley Research Center Design. CAD Model cutout showing secondary chamber with curved exhaust duct (left) and CFD model that was used to get scaled dimensions (right)

A CAD rendering of the final dual Hartmann generator prototype used for testing is shown in **Figure A3**. The prototype did not fully optimize the sizing of the chamber and the horn, and several adjustability features were incorporated. It is anticipated that significant gains in compactness will be made in future iterations.

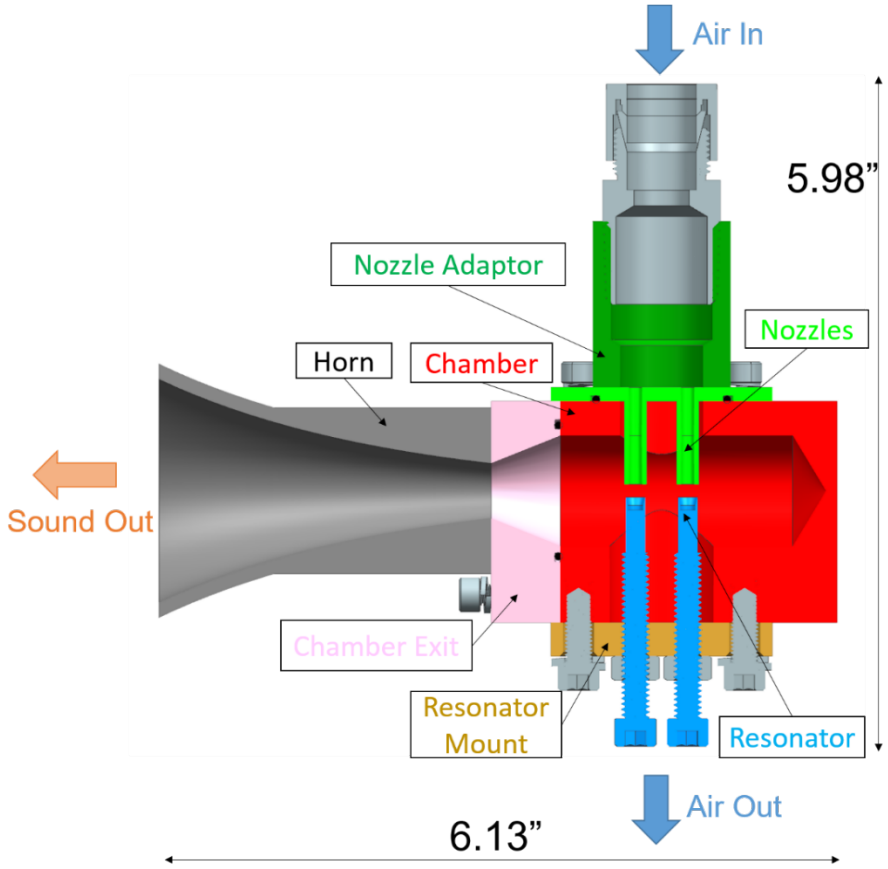

Figure A3: Final CAD rendering of the prototype dual Hartmann generator.

Nozzle and Resonator Design

Optimization of the design parameters came from research on Hartmann generator literature. Kastner and Samimy [20] showed that resonator diameter D_r should approximately equal resonator length L_r for short tubes, and that nozzle diameter D_n should approximately equal resonator diameter as well.

The nozzles were designed as converging-diverging nozzles to achieve supersonic flow, as shown by [20],[22]. Supersonic flow and operation in the Jet Regurgitant Mode (see [19, Table 3]) is preferred as Kastner and Samimy [20] show a correlation between higher Mach number and higher SPL.

Resonance in a Hartmann generator is determined by the placement of the resonator within the jet, and thus the nozzle-resonator spacing, S/D_n. Raman and Srinivasan [19, Figs. 8,9], Kastner and Samimy [20, p. 1930], and Raman et al. [22, Fig. 6] all describe studies that with a supersonic nozzle, the ideal S/D_n is in the range of 1-2, preferably closer to 1.0. Further, the nozzle pressure ratio (NPR), which determines the nozzle exit Mach number, is a key factor in which acoustic mode is achieved [19] and what size and shape the jet takes. Benchtop tuning of these parameters was performed to achieve the goals of two-tone operation with maximum SPL. A diagram of key geometric parameters is shown in **Figure A4**

To enable this, the resonators were machined from bolts, allowing for a built-in adjustability to the nozzle-resonator spacing during benchtop testing. A pressure regulator was employed to control the upstream pressure.

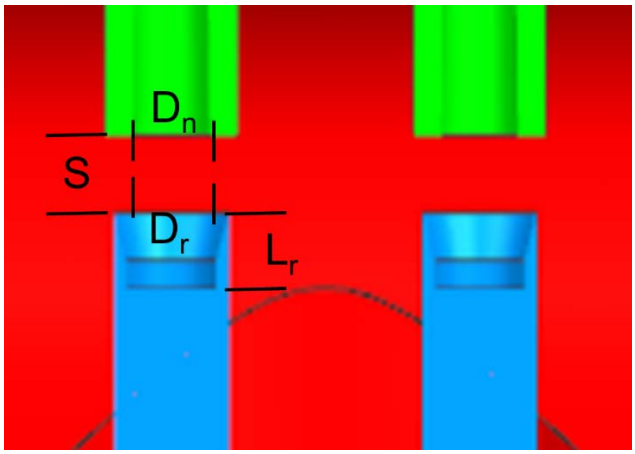

Figure A4: Geometric parameters for the nozzle and resonator of the dual Hartmann

Figure A5 shows the resonator schematic. Narayanan et al. [21] showed that an internal chamfer of 15 degrees produced the highest SPL between the options investigated. Due to the known deficiencies of equation A1 for short resonator tubes, four resonators of varying depths were made with the intention of testing and utilizing an iterative design approach two select a suitable pair of resonators.

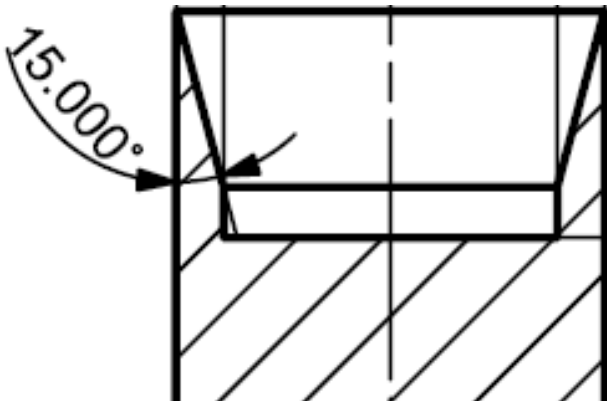

Figure A5: Resonator design, showing internal chamfer of 15 degrees. Overall length L_r varies.

The nozzle-resonator apparatus included two other features for risk reduction. First, due to a concern about the possibility of twin-nozzle coupling (see Seiner [18]), the nozzles were spaced laterally further than otherwise necessary. The coupling phenomena is observed to occur at nozzle separations of 2.5 D_n or less. Such a coupling would result in a single tone. A design separation of 4 D_n was employed to successfully mitigate this risk. Alternatively, Seiner offers creation of a small tab or other discontinuity in one of the nozzle exits to interrupt the coupling phenomenon, a step that was unnecessary in this case. Second, with two Hartmann generators in the chamber, there were multiple possible orientations within the chamber, as illustrated in **Figure A6**. The design allowed for two orientations to be tested as candidates. The 'front-to-back' orientation keeps both nozzle-resonators in line with the acoustic port but could potentially result in acoustic shielding of one generator by the other. The 'side-to-side' orientation solves the acoustic shielding problem at the cost of having neither nozzle-resonator aligned with the acoustic port.

Figure A6: Nozzle-resonator orientations tested on the dual Hartmann.

Acoustic Horn Design

The acoustic horn shown in **Figure A7** had been used in earlier Hartmann generator studies. A comparative study was conducted to determine the necessity of a horn and if so, which of several designs maximized SPL. The existing horn was not believed to be ideal for the ~21 kHz tonal frequencies. An array of additional designs was additively manufactured by Teja Sathi, an undergraduate researcher. Two of these new prototypes are shown in **Figure A8**.

Figure A7: Acoustic horn additively manufactured for use with earlier Hartmann generator

Figure A8: New acoustic horns additively manufactured as candidates for the dual Hartmann generator: Exponential with circular cross-section (left) and exponential with rectangular cross-section (right)

Benchtop Tests

Upon manufacture of the prototype, several series of benchtop tests were performed to determine proper resonator placement and verify overall operation of the dual Hartmann generator. Individual resonators in the chamber were verified for tonal operation. Different orientations of the nozzle-resonator assembly were tested to verify two-tone operation and signal strength. Different combinations of resonators were then used to determine a pair that operated at high SPL and at a low beat frequency, f_b. The proper nozzle-resonator spacing in terms of S/D_n and proper nozzle pressure ratio were determined throughout via manual tuning. Several newly designed acoustic horns were tested to compare to a previously manufactured acoustic horn.

Individual resonator response

Each of the four manufactured resonators was tested individually to measure tonal response. Tuning was required to get tonal responses near the predicted frequency shown in **Table A1**. Each

resonator responded best at a 45 psig upstream (approximately 4.2 NPR), with spacing of 1.0 S/D_n. The predicted values are from the quarter-wavelength formula (Equation A1).

Resonator Orientation

As shown in **Figure A6**, two possible orientations of the dual Hartmann generator assembly are rotationally possible. Benchtop testing determined that the "side-by-side" orientation produced relatively lower output levels, thought to be due to non-alignment of the generators with the acoustic port. The "front-to-back" orientation did not exhibit any negative acoustic shielding effects, with the levels of both tones measured clearly.

Resonator Pairings

With both generators operating, output was evaluated to look for the presence of two distinct tones at the expected frequencies, with a key parameter being the output f_b. In the dual configuration, the quarter-wavelength formula was fairly accurate in predicting the produced frequencies, with approximately a 0.5 kHz mismatch across the board. Thus, the pairings approximately produced what was predicted by **Table A2**, and it was trivial to select the closest pairing of tubes A and B.

Table A1: Resonator tubes made, with cavity lengths, L and predicted* frequency of tonal output

Tube	L (in)	f (kHz)*
A	0.120	20.9
B	0.116	21.5
C	0.108	22.6
D	0.094	24.9

Table A2: Tube pairings along with predicted* beat frequency, f_b (absolute frequency difference)

Pairing	Beat f (Hz)*
A+B	600
B+C	1100
A+C	1700
C+D	2300
B+D	3400
A+D	4000

Nozzle Pressure Ratio (NPR) and Spacing, S/D_n

Benchtop tuning and testing showed that a 2.0 S/D_n occasionally produced a tonal response in individual resonators, albeit at a different frequency than predicted and with a lower SPL than with 1.0 S/D_n. At a given S/D_n, the upstream pressure was adjusted until live measurements confirmed the presence of ultrasonic tones. Often, this was in the range of 40-65 psig (3.9 – 5.6 NPR). Ultimately, benchtop tuning set the gauge pressure at 45 psig approximately 25 feet upstream of the dual Hartmann air inlet. The hose used had a 0.5" tube diameter, and losses between the pressure gauge and the nozzle were expected to be low. Test-to-test and day-to-day variation of the ideal gauge pressure varied by ± 1-2 psi. Overall, the NPR that resulted in correct operation was around 4.2

Horn Testing

The acoustic horn candidates were measured using an array of microphones to determine sound pressure drop off with emission angle. The hornless configuration performed poorly relative to the horn configurations, all of which exhibited similar performance, as shown in **Figure A9**. The two datapoints for each horn represent the SPL at each of the two tones. Due to the similar performance of the three horns, the existing horn was chosen to incorporate into the final design. The existing horn was manufactured with high temperature plastic and would not have to be remade prior to utilization in engine testing.

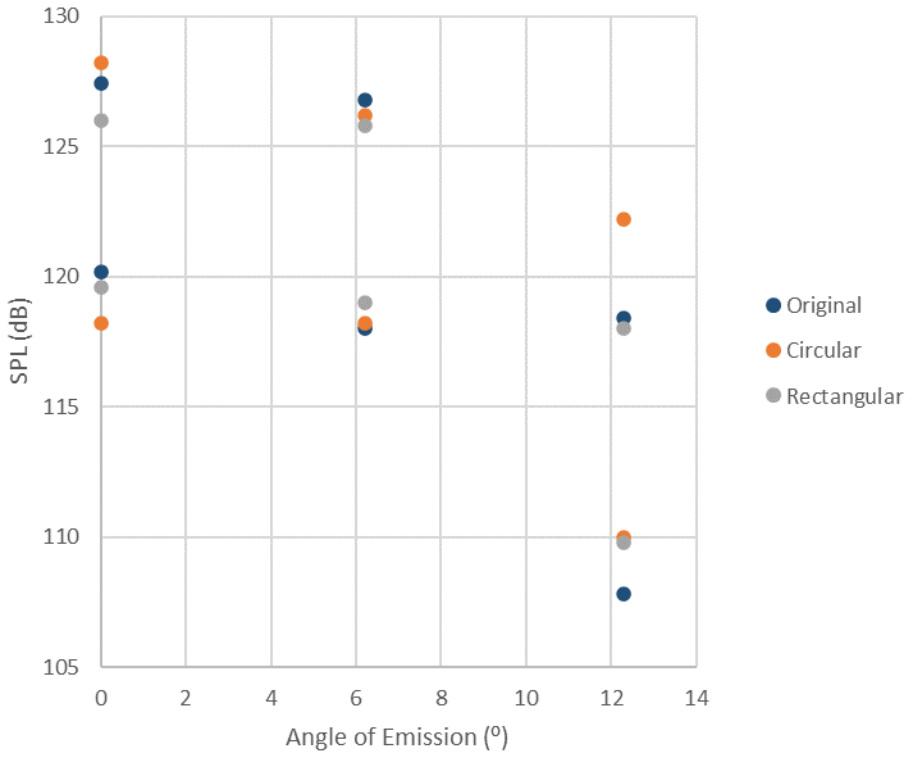

Figure A9: Sound Pressure Level (SPL) vs. Emission Angle for three horn candidates. Each of the two datapoints represents SPL at a different one of the two tones.

Final prototype configuration

Upon identifying the ideal resonators, orientation, spacing, and pressure ratio, a two-part epoxy was used to lock the resonator bolts in place. The final configuration values are given below:

Resonator A: L_r/D_n = 1.02, producing a ~20.5kHz tone
Resonator B: L_r/D_n = 0.98, producing a ~21.0kHz tone
Beat frequency: ~500 Hz, less than the ~600 Hz estimated value
Orientation: "Front-to-back", as seen in Figures A3 and A6
Spacing: S/D_n = 1.0 for both resonators
Nozzle Pressure Ratio: 45 psig upstream of the ~25' long 0.5" diameter feed tube into the dual Hartmann, or an NPR of 4.2.

Figure A10 shows the realized prototype. This image was taken prior to the resonators (middle two bolts in the bottom of the image) being epoxied in place. The overall dimensions are approximately 6"x6"x2".

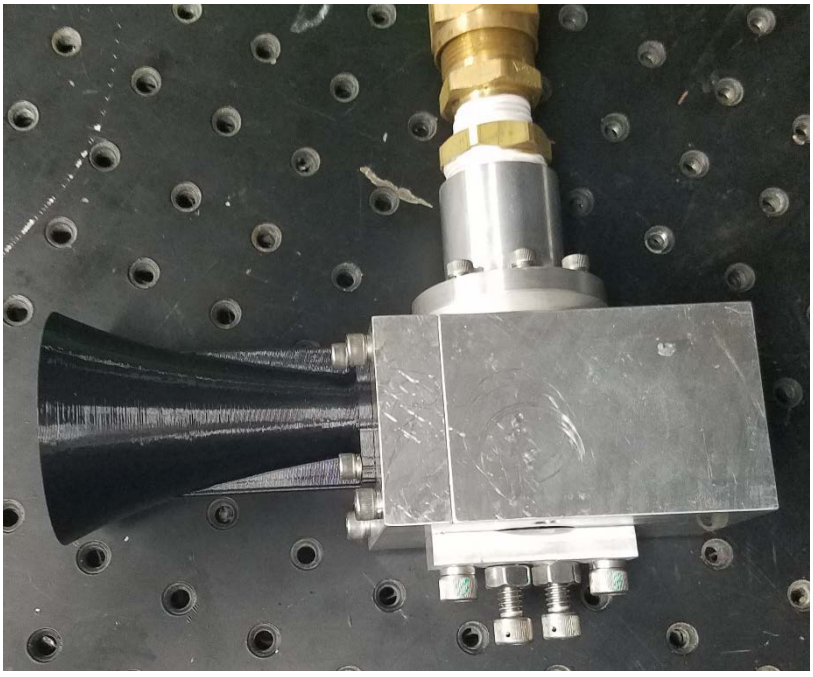

Figure A10: Photograph of the realized dual Hartmann prototype.

This prototype does have the potential to be reduced in size considerably. Removing the adjustability features, optimizing the secondary chamber size, shrinking the horn, and optimizing the air supply are all potential avenues for overall size reduction. This will be necessary for future applications.

Appendix B: Time Delay Estimation approach development

Cross-correlation, the classic method of TDE, was successfully used both during benchtop experiments [2-4] and a prior jet experiment [5], due to the nature of the spark source signal used in those experiments. Naturally, initial attempts of TDE processing on the dual Hartmann TFE731 engine experiments were with cross-correlation. The cross-correlation approach was found to be unsuccessful, failing to achieve adequate resolution of correlation peaks, as demonstrated in **Figure B1**. The inadequate resolution resulted in ambiguity in choosing the correct time delay estimate, potentially with a large estimation error, or anomaly, being chosen. This problem became the central objective behind a new approach to data processing. The anomaly problem is discussed in [15, 17] Attempts to reduce anomalous selction were made with a variety of alternative data processing techniques, following several approaches found in the literature.

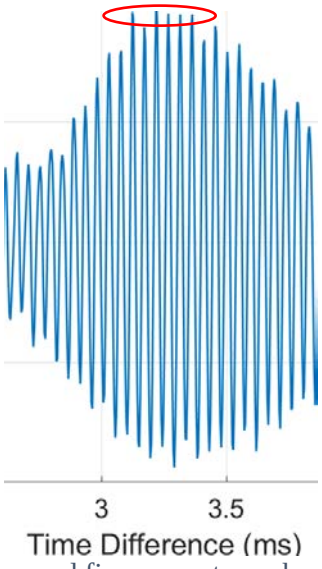

Figure B11: Cross-correlation reveals around five separate peaks or near-peaks of the correlation coefficient. This makes selecting the true TDE difficult.

The Generalized Cross-Correlation (GCC) approach of Knapp and Carter [9] combines several processing approaches into one framework, each differentiated by a processor, or weighting function. Knapp and Carter examined a variety of processor functions, both new and old, with varying strengths and weaknesses for each. The comparison of processors is shown in Table 1 and discussed in Section 2C.

Least-mean-square adaptive filtering models the signal delay as a FIR filter and finds the coefficients of that filter to minimize the error signal. Chern and Lin [24] provide an evaluation of such an approach. One of the noted areas where the above method fails is when the noise signals at two receivers, $w_1(n)$ and $w_2(n)$, are correlated and SNR is low. In the jet engine environment, unfortunately, both statements are true. Samples of the data from the TFE731 engine test were passed through an LMS filter like the one described by Chern and Lin without success.

Bispectrum methods use third order cumulants to detect similarities between the signal to estimate time delay. Nikias and Pan [25] describe an improved algorithm that takes advantage of the bispectra property of “preserving information of non-Gaussian stationary random processes” while

removing additive noise that is assumed to be stationary Gaussian. The issue with the application to the jet noise problem is the non-Gaussian nature of the noise components. Several representative samples of jet noise alone at two spatially distant microphones revealed non-zero skewness, indicating that the noise is not Gaussian. As such the higher order spectra are *not* identically zero and thus do not drop out of the bispectrum TDE equations [25, equation 17]. Attempts to implement the algorithms in the paper produced erroneous results, confirming that the non-zero noise-signal cumulants have a significant impact on the result. This was true for both the direct and indirect computational methods.

Comparisons of Methods

Zhang and Abdulla [26] present a comparative study that discusses a wide range of TDE methods, including several that were not implemented on TFE731 engine data. The study looks at both a simulated dataset as well as actual noise. Primarily, this study compares three GCC processor methods (standard cross-correlation (SCC), Phase Transform (PHAT), and Maximum Likelihood (ML)) along with the average square difference function (ASDF) method. The ASDF method finds the squared difference between signals as a function of τ, and thus requires no computation in the spectral domain. Zhang and Abdulla found this to work best in a simulated domain, but with real data, PHAT performed best as SNR decreased [26, Section 5].

Similarly, this paper has compared the same three GCC processor methods as Zhang and Abdulla. Similarly, in application on the TFE731 dataset, the PHAT processor was found to best reduce TDE anomalies. The reason for the relative success of the PHAT is that it counteracts the haystacking phenomena as discussed in Section 2B. While the GCC approach in general is known to suffer from inaccuracies if the noise components are correlated, the advantage of the PHAT outweighs that disadvantage.

GCC and PHAT – Additional Notes

Knapp and Carter [9] focus on the Maximum Likelihood (ML) processor, as they show that it minimizes variance to a value arbitrarily close to the Cramér-Rao Lower Bound (CRLB). The CRLB is a bound on the minimum variance achievable. However, Scarbrough [16] emphasizes that the CRLB is difficult to achieve in practice, as it requires an unknown “sufficiently long” sampling length. Scarbrough compares a number of different alternative estimates of correlation performance, including the Correlator Performance Estimate (CPE) and Ziv-Zakai Lower Bound (ZZLB). For many signals of interest, particularly at low SNR, a complete statistical description of the signal and noise is necessary to compute these more realistic metrics of variance. Scarbrough shows that each of the processors performs similarly at low SNR for a simulated signal. Thus, the recommended approach is to use directed experimentation as to which signal processor works best, by applying some knowledge of the signal and problem domain.

This is shown for three of the processors in the paper, in Section 4. Another approach is to examine the processor equations themselves and consider domain knowledge. To begin, consider the ML processor, Equation B1:

$$\psi(f) = \frac{|\gamma_{12}(f)|^2}{|G_{x_1,x_2}(f)|(1-|\gamma_{12}(f)|^2)} \quad \text{(B1)}$$

This processor includes terms for the magnitude-squared coherence, $|\gamma_{12}(f)|^2$. For many signals of interest, coherence weighting makes sense as a method to filter out uncorrelated noise, as the signal coherence will be high only for the signal components. In the jet engine environment, the haystacking phenomena serves to modulate the phase across turbulent shear layers. One effect this has is to greatly deteriorate coherence between the sent and received signals. Thus, the ML processor is essentially weighting by a corrupted function, as the coherence is not very great between the sent and received signals suffering from severe haystacking.

If both terms that contain the magnitude-squared coherence are removed as a weighting component, the following processor is obtained (Equation B2):

$$\psi(f) = \frac{1}{|G_{x_1,x_2}(f)|} \quad \text{(B2)}$$

Equation B2 is exactly the PHAT processor, which weights by the cross-power spectral magnitude. As such, there is no surprise when a trial-and-error approach demonstrates the superior results from using the PHAT processor.

Appendix C: GCC Comparison at N_{1Corr} = 50% to 70%

The primary focus of a detailed comparison of processors were the SCC, ML, and PHAT methods. Processors such as the SCOT and Roth were only processed for a small subset of cases and are unavailable for direct comparison. From observation, these processors performed similarly to the ML in some cases and to the PHAT in others. As noted in the paper, the PHAT performed well in this case relative to the other processors, but not so much so that it is recommended to the exclusion of processing a subset of the data with a range of processors.

N_{1Corr} = 50%

At the N_{1Corr} = 50% engine condition, the modulating dual Hartmann tones result in an SCC that is in the correct range of values, as designed, but with numerous ambiguous peaks in the vicinity. The ML correlations originally suffered from low frequency trends in the correlations that skew the results for many of the microphones. Various high-pass filters did not improve the results significantly. The ML processed data shown reflect the application of a high-pass filter.

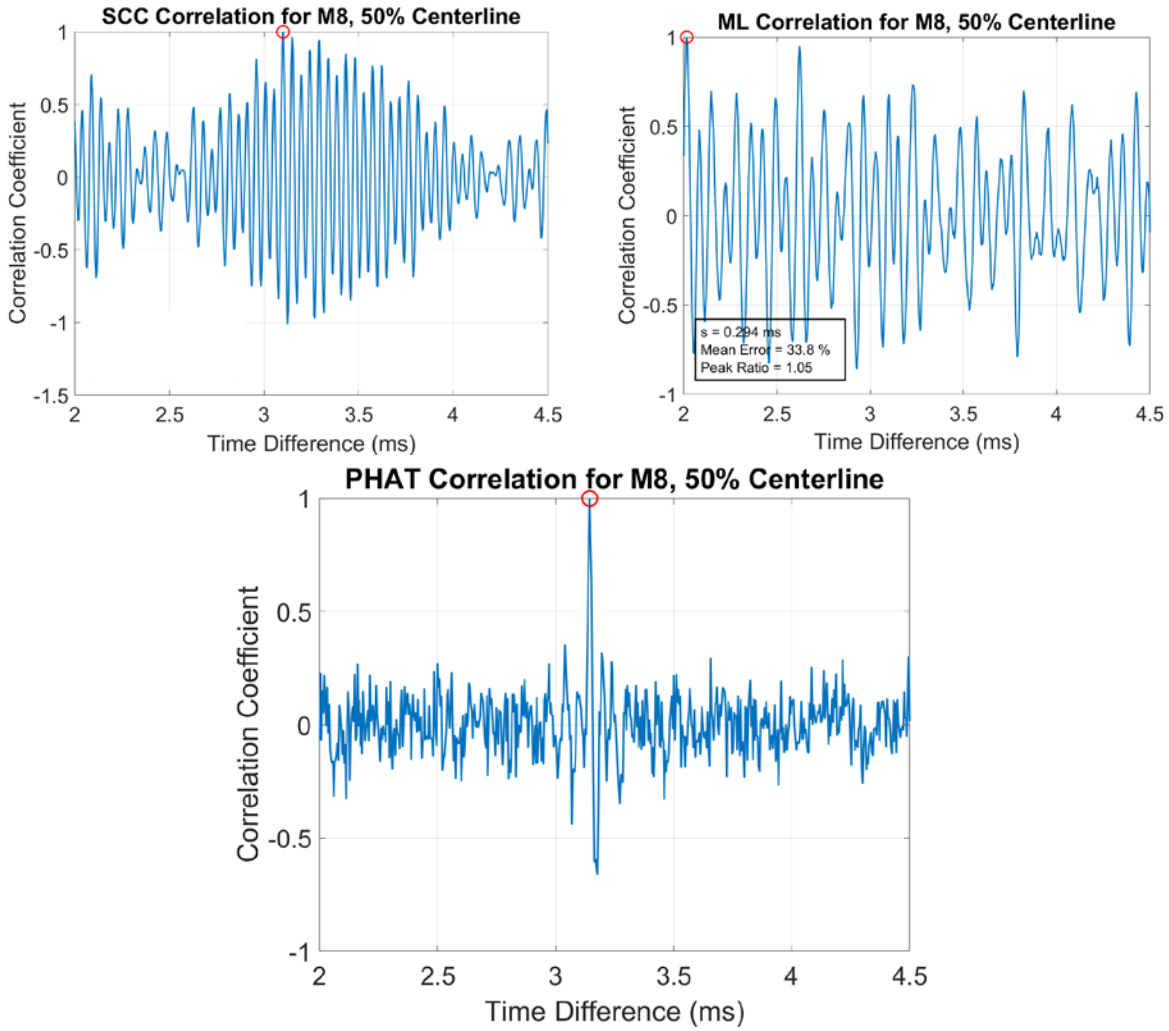

Figure C12: Three correlation functions (SCC, ML, and PHAT) at the N_{1Corr} = 50% engine condition, M8.

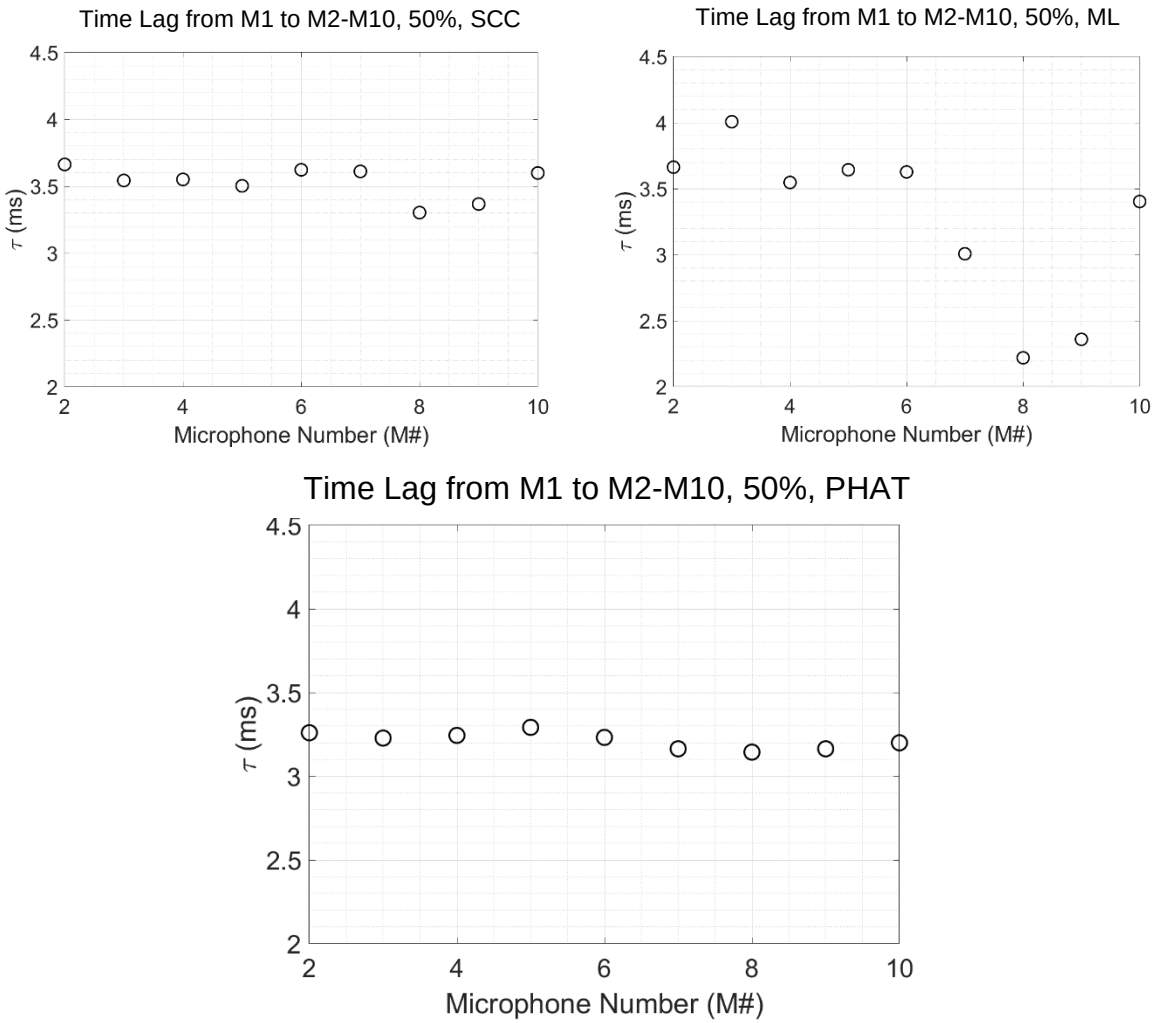

Figure C13: Three correlation functions (SCC, ML, and PHAT) at the N_{1Corr} = 50% engine condition. Note: τ values may differ from method to method due to some charts being processed with a Δt constant offset applied. Similarly, comparisons to **Figure C12** may differ by a Δt. Comparisons within each chart are valid, while comparisons between different charts may not be.

N_{1Corr} = 60%

At the N_{1Corr} = 60% engine condition, the issues affecting each processor are similar to those in the 50% case. The ML correlations display an increasing probability of having an anomalous peak far from the vicinity of the true TOF.

For the PHAT, M10 appears to be the only truly anomalous result. The correlation for M10 is shown in **Figure C16**, which makes an excellent case for the smarter "peak-finding" approach described in Section 5C of the paper.

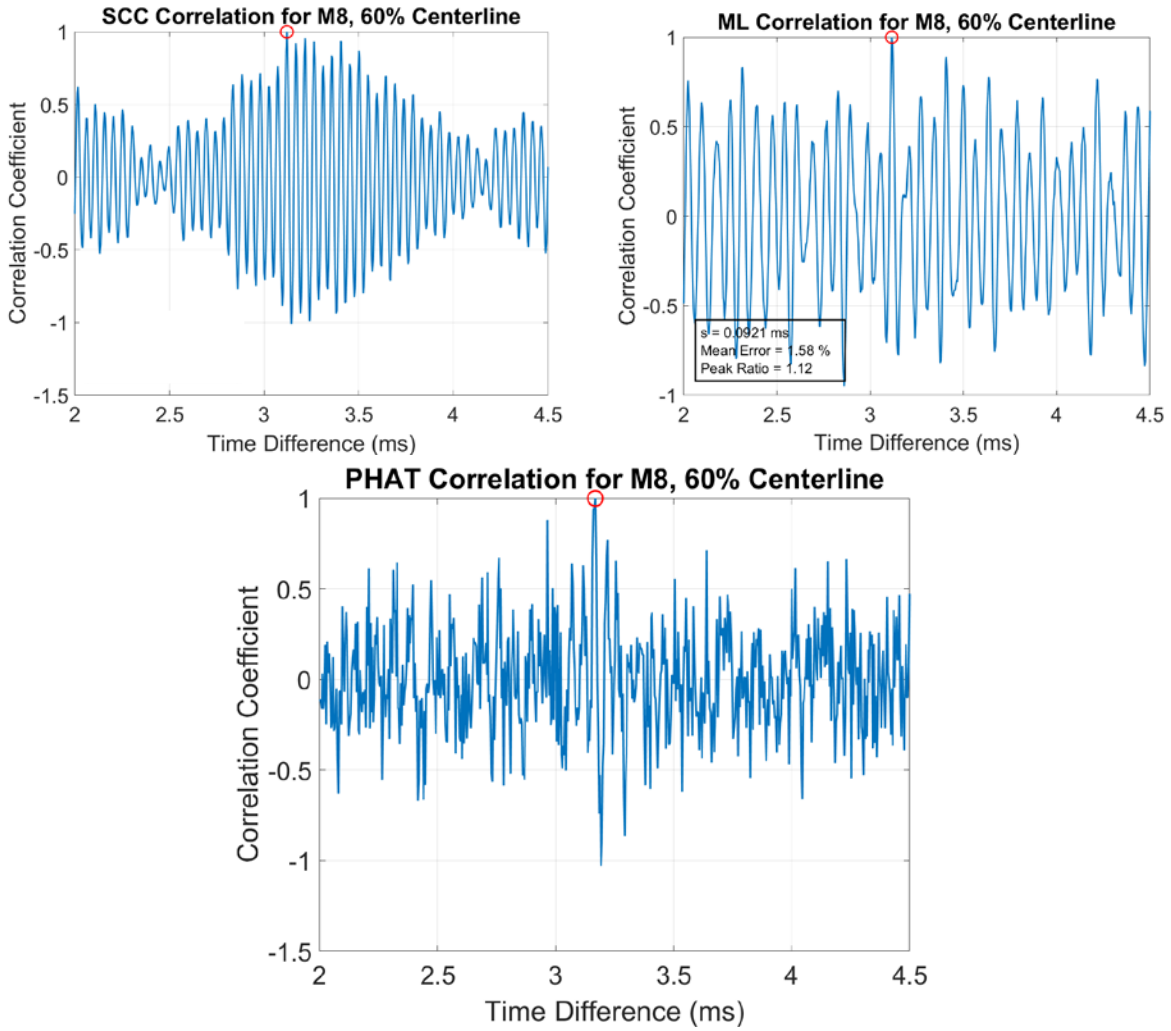

Figure C14: Three correlation functions (SCC, ML, and PHAT) at the N_{1Corr} = 60% engine condition, M8.

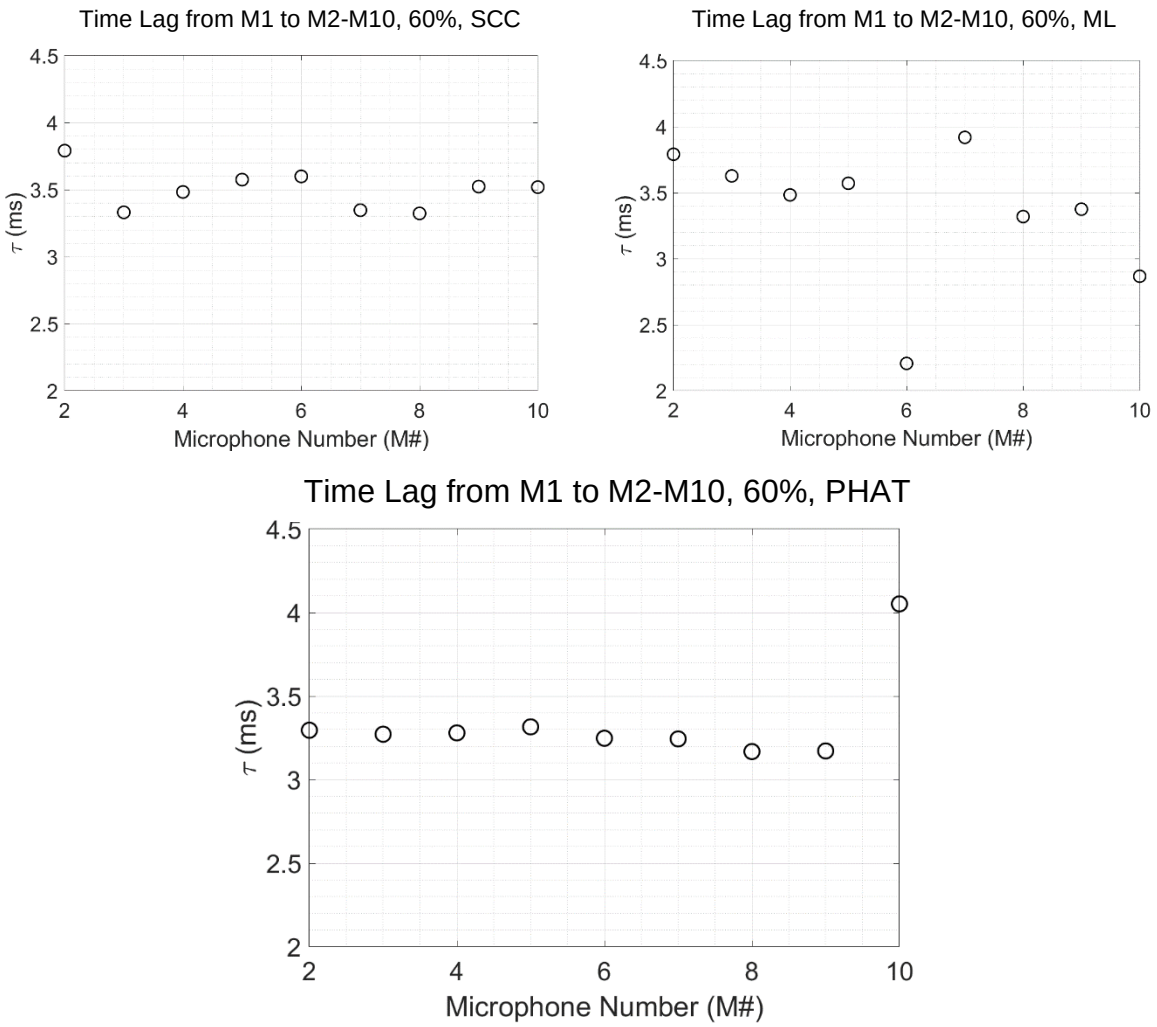

Figure C15: Three correlation functions (SCC, ML, and PHAT) at the N_{1Corr} = 60% engine condition. See note in.

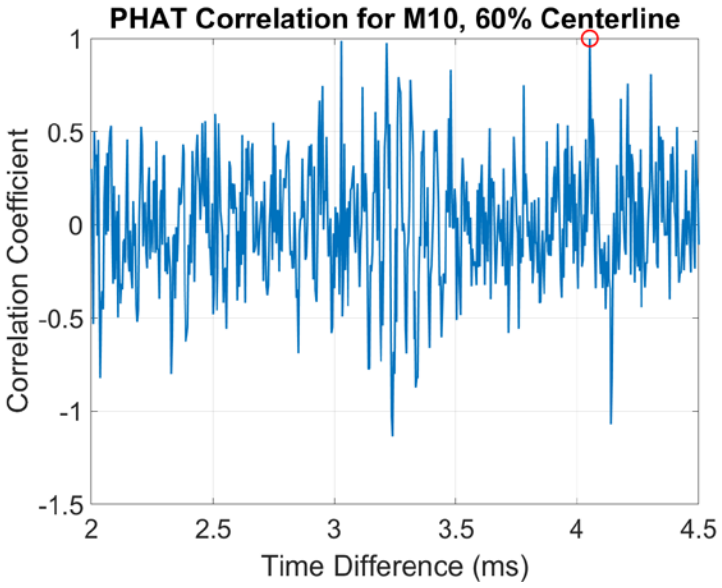

Figure C16: PHAT correlation at N_{1Corr} = 60%, M10. Note the near 1.0 correlation coefficients near 3.0 ms and 3.25ms. Based on the nearest neighboring microphone, one of these, particularly 3.25ms, is likely to be the true time lag, τ.

N_{1Corr} = 70%

At the N_{1Corr} = 70% engine condition, it is unsurprising that the TDEs are in a wider and wider band, and the TDE from the SCC and ML are scattershot compared to the PHAT, as seen in **Figure C18**. In the case of the ML correlation, the signal coherence is quite low, resulting in much less weighting of the signal compared to the noise components, and the correlation is virtually meaningless, hence TDEs across the entire range of the time lag window.

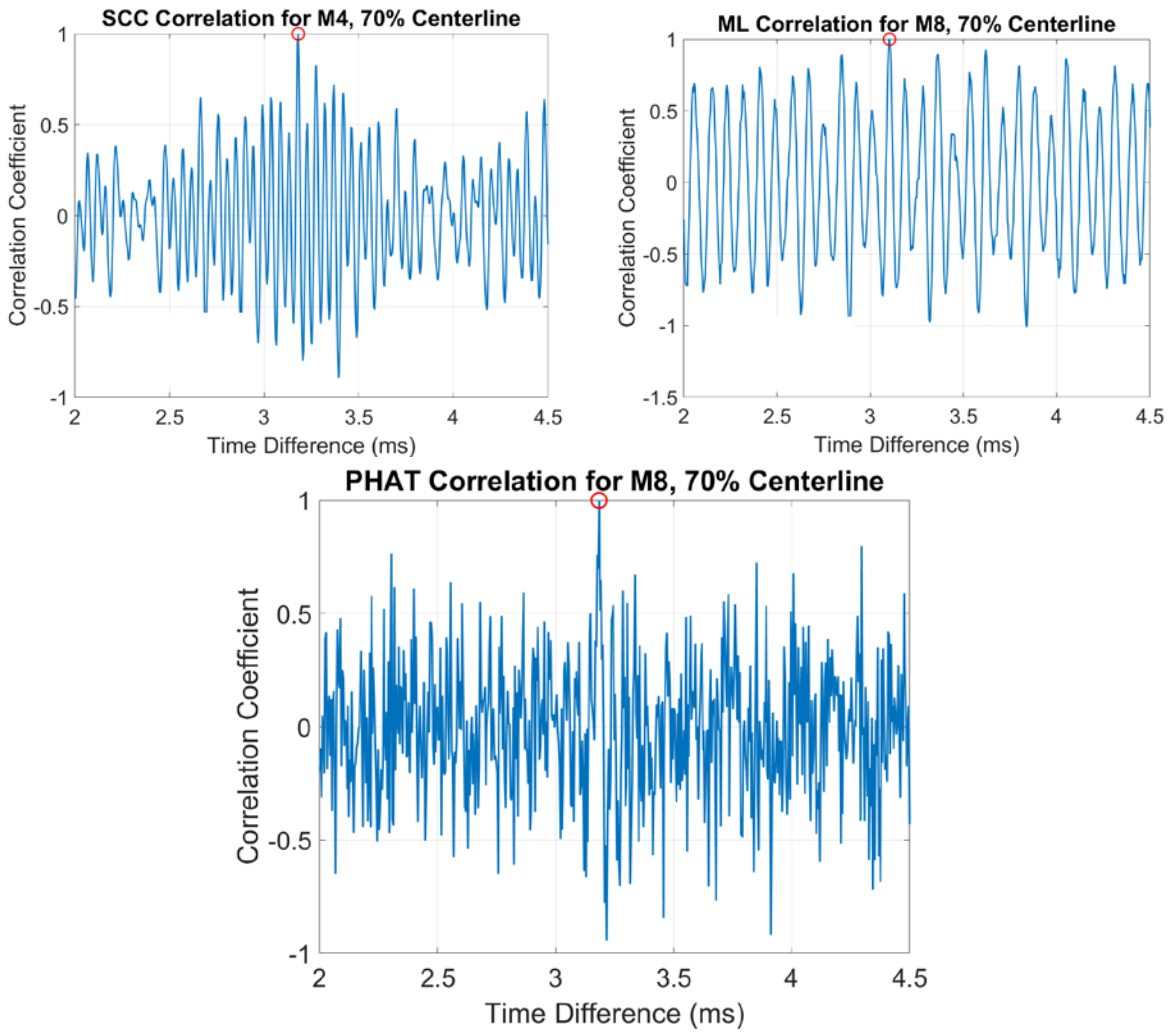

Figure C17: Three correlation functions (SCC, ML, and PHAT) at the N_{1Corr} = 70% engine condition, M8.

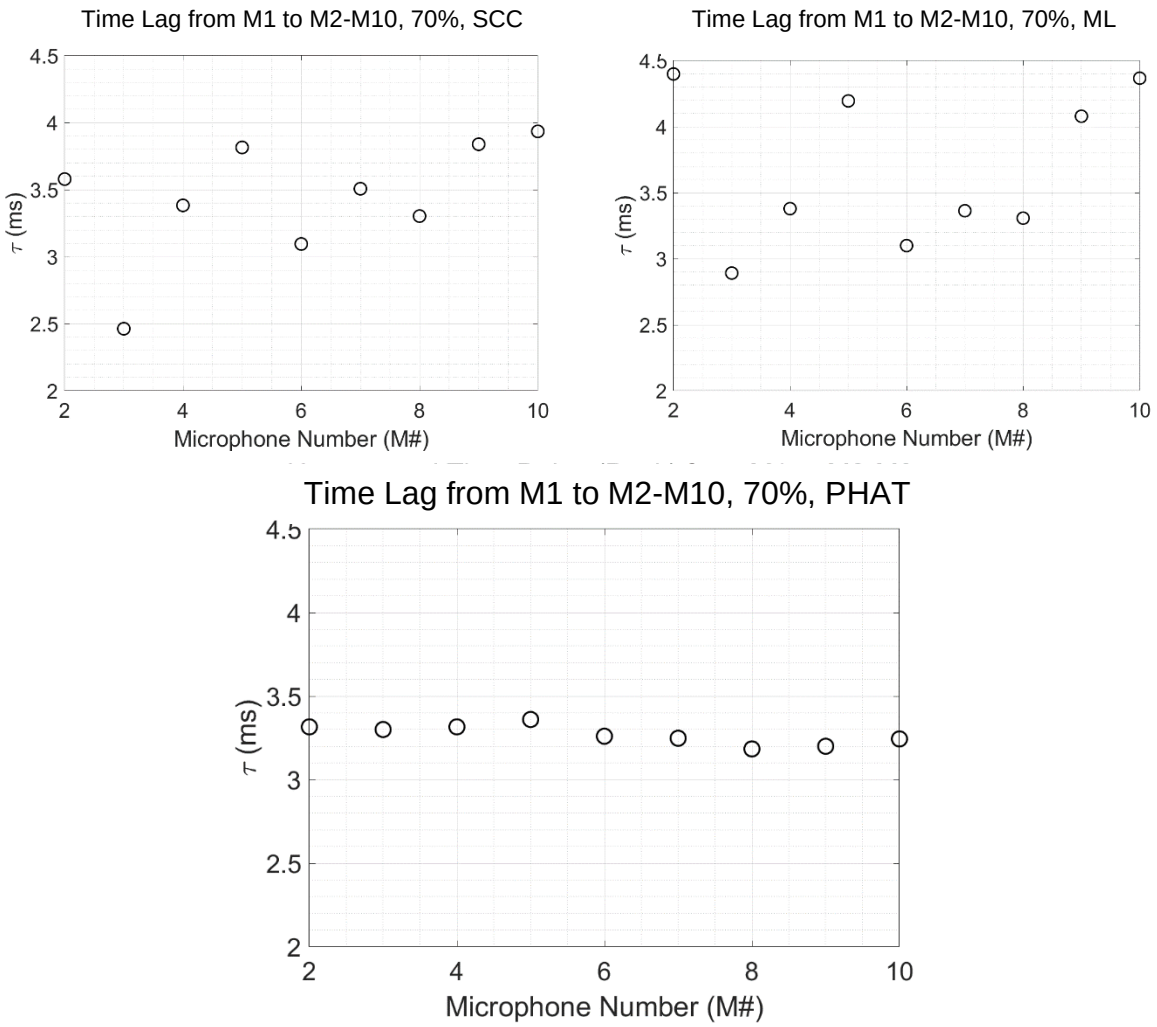

Figure C18: Three correlation functions (SCC, ML, and PHAT) at the N_{1Corr} = 70% engine condition.

Appendix D: Expected TOF Values - Ambient

In the ambient condition, the expected TOF for each microphone can be found in a straightforward manner using the geometry of the source and receiver position, with a correction for the source to reference microphone distance. Referring to **Figures 7** and **8** as a reference for the approximate dimensions, and using M2 as an example, we have a 4 in. (10.16 mm) offset in the vertical direction, a 7 11/16 in. (19.526 mm) offset in the axial direction, and a 49 in. (124.46 mm) cross-stream distance.

$$d_{M2} = \sqrt{dx^2 + dy^2 + dz^2} \tag{D1}$$

$$d_{M2} = \sqrt{124.46^2 + 10.16^2 + 19.526^2} = 126.4\ mm$$

The source to reference microphone distance is 3 in. (7.62 mm), and with a speed of sound, c, of 345.1 m/s at an ambient temperature of 23.3 ºC, the expected time delay is given by

$$TDE_{0-2} = \frac{(d_{M2} - d_{M0})}{c} \tag{D2}$$

$$TDE_{0-2} = \frac{(126.4\ mm - 7.62\ mm)}{345.1\ m/s} = 0.3442\ ms$$

Figure D19 shows the expected time delay, alongside the observed time delay, for each of the nine microphone pairings with M1.

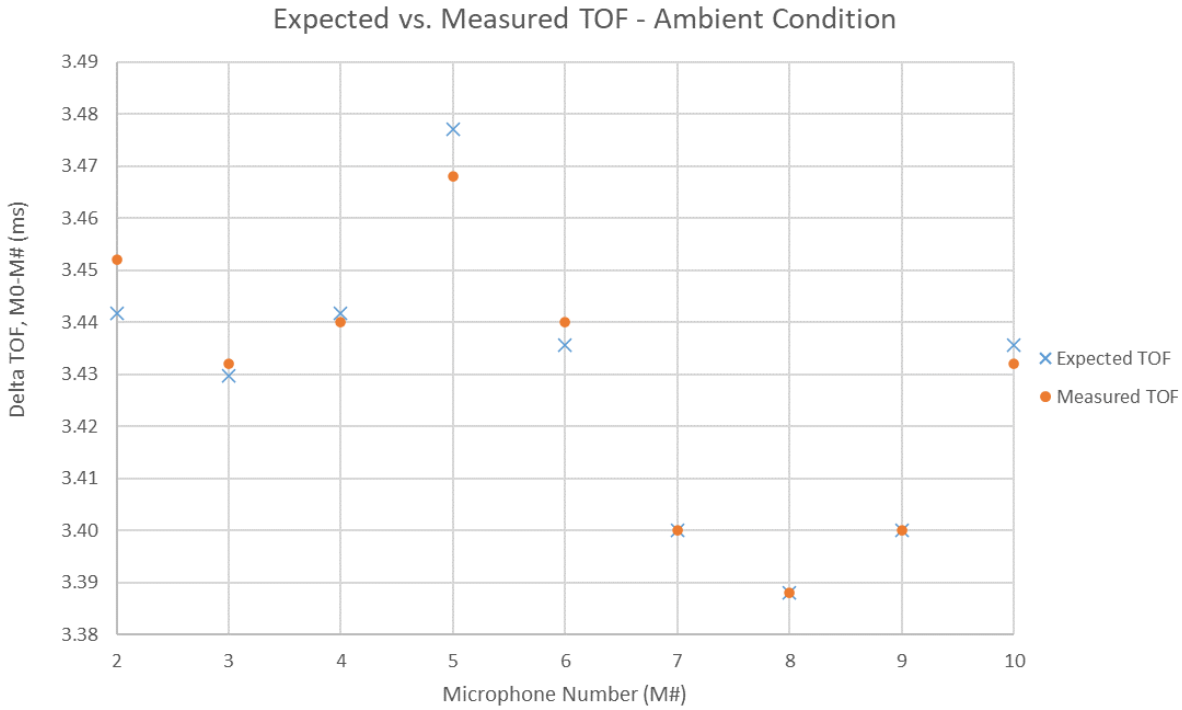

Figure D19: Expected vs. Measured TOF for the Ambient Condition.

The values were derived from the nominal dimensions of the experimental set-up. The average error in the TDE values is 0.10%. One potential source of error could be due to slight geometric measurement errors of the position of the microphone array. By adjusting the values of dx, dy, and/or dz by uniform amounts across all pairings, a lower average error can be achieved. This suggests a slight positioning error is present in the data, and can be adjusted for on the basis of the ambient measurements. As tomographic measurements require source and receiver spatial positions as well as TDE, this is a useful method to reduce the influence of manual geometric measurements of the test equipment.

Appendix E: MATLAB Codes

The following MATLAB code is the '**Main**' program for setting parameters, loading the desired data files, displaying snippets of raw time series data, displaying spectra, and plotting correlation results. The code that follows is called '**gcc_sample_ave**', which takes in a 250000 x n pair of vectors of vectors that contain the 250,000 sample points for each 1 second sample of data. Each of the n 1 second samples are then used to produce an overall correlation function, as described in Section III of the paper.

Main

```
%% Startup
clear;close all; clc;
addpath(genpath('C:\Users\kasilas\Documents\MATLAB\RO_FUNCTIONS'));
run('FTN_SET_PLOTFORMAT.m')

%% Inputs and Parameter Setting - User Adjusted
%options:
test_name = "tfe731";
engine_case = "50% Cent"; %Set here
com_spectra = 0;  %Compute Spectra?
com_tref = 0; %Compute tref?
com_TOF = 1;  %Compute TOF?

%DEFAULT AND/OR SET VALUES
% Set to 'Station' if files in test_series are 'Station_#_Sample_#' format,
%'Data' if files are in "Data_#" format, 'Sample' if in "Sample_#" format.
sta_samp = 'Sample'; %Default only; reset below

%ONLY OPTIONS THAT SHOULD BE ADJUSTED - PROCESSING
sam_per_sta = 120;
gcc_method = 'PHAT';
numseg = 9;
filter = 'off';
%ONLY OPTIONS THAT SHOULD BE ADJUSTED - PROCESSING

%Figure Sets:
% 1-11: Time Series, 10 ms
% 12-22: Spectra; Measured Gains
% 23-32: Correlations
% 33+: Stations

if test_name=="jt15d"
    amb_temp = 275; %Ambient temperature in Kelvin
    ref_mic_id = 0;
    num_mics = 10; %Not counting reference mic
    mic_range = 1:10;
    mic_array_offset = 1;
    folder='C:\Users\kasilas\Documents\MATLAB\Data\';
    num_stations = 43;
    sta_start = 1;
    gain = [0.001046 0.00084815 0.0012115 0.0009397 0.0008856 0.0007826
0.00084695 0.002192 0.002459 0.0010075 0.0008323];

    horn_angle = 12;
```

```
    switch engine_case
        case 'Noise'
            sta_samp = 'Sample';
            test_series = 'JetNoise\';
            if (sam_per_sta > 45)
                sam_per_sta = 45;
            end
        case 'Ambient'
            sta_samp = 'Sample';
            test_series = 'Ambient\';
            horn_angle = 2;
            if (sam_per_sta > 30)
                sam_per_sta = 30;
            end
        case 'Idle_Cent'
            sta_samp = 'Sample';
            test_series = 'Idle_Centerline_2deg\';
            horn_angle = 2;
            if (sam_per_sta > 30)
                sam_per_sta = 30;
            end
        case '50_Cent'
            sta_samp = 'Sample';
            test_series = '50_Centerline_7deg\';
            horn_angle = 7;
            if (sam_per_sta > 32)
                sam_per_sta = 32;
            end
        case '65_Cent'
            sta_samp = 'Sample';
            test_series = '65_Centerline_12deg\';
            horn_angle = 12;
            if (sam_per_sta > 32)
                sam_per_sta = 32;
            end
        case '80_Cent'
            sta_samp = 'Station';
            test_series = '80_Traverse\';
            num_stations = 1;
            sta_start = 18;
            horn_angle = 12;
            if (sam_per_sta > 30)
                sam_per_sta = 30;
            end
        case '80_All'
            sta_samp = 'Station';
            test_series = '80_Traverse\';
            num_stations = 43;
            sta_start = 1;
            horn_angle = 12;
            if (sam_per_sta > 30)
                sam_per_sta = 30;
            end
    end
else
    amb_temp = 296.5; %Ambient temperature in Kelvin
    ref_mic_id = 1;
```

```
    num_mics = 9; %Not counting reference mic
    mic_range = 2:10;
    mic_array_offset = 0;

folder='C:\Users\kasilas\Documents\MATLAB\Data\Data_Sept_25_Centerline_Test\'
;
    sta_samp = 'Sample';
    num_stations = 1;
    sta_start = 1;
    gain = [0.0010075 0.0009397 0.002459 0.00084695 0.0007826 0.0008856
0.002192 0.0008323 0.00084815 0.001046]; %Mics 1-10
    switch engine_case
        case 'Ambient'
            sta_samp = 'Sample';
            test_series = 'Ambient\Hartmann\';
            if (sam_per_sta > 12)
                sam_per_sta = 12;
            end
            name_case = "Ambient Conditions";
        case 'Idle'
            sta_samp = 'Sample';
            test_series = 'Idle\Hartmann\';
            if (sam_per_sta > 120)
                sam_per_sta = 120;
            end
            name_case = "Idle (~30%) Centerline";
        case '50% Cent'
            sta_samp = 'Sample';
            test_series = '50pct\Hartmann\';
            if (sam_per_sta > 120)
                sam_per_sta = 120;
            end
            name_case = "50% Centerline";
        case '60% Cent'
            sta_samp = 'Sample';
            test_series = '60pct\Hartmann\';
            if (sam_per_sta > 120)
                sam_per_sta = 120;
            end
            name_case = "60% Centerline";
        case '70% Cent'
            sta_samp = 'Sample';
            test_series = '70pct\Hartmann\';
            if (sam_per_sta > 120)
                sam_per_sta = 120;
            end
            name_case = "70% Centerline";
        case '80% Cent'
            sta_samp = 'Sample';
            test_series = '80pct\Hartmann\';
            if (sam_per_sta > 120)
                sam_per_sta = 120;
            end
            name_case = "80% Centerline";
    end
end
%% Inputs - Fixed or Relatively Fixed
```

```
FS=250000; %Sampling rate
duration=1;  %Signal length in seconds

camb = sqrt(1.4*amb_temp*8314/28.97);
pref = 2*10^-5; %reference pressure
tref = 0;

%% Convert tdms files to .mat file (if necessary)
extension='*.tdms';
fileinfo = dir(strcat(folder,test_series,extension));
numfiles=length(fileinfo);
for count=1:1:numfiles
    filename=strcat(folder,test_series,fileinfo(count).name);
    if exist(strcat(strrep(filename, '.tdms', '.mat')), 'file') ~= 2
        FTN_CONVERT_TDMS_SIMPLE(strcat(filename), 1);
    end
end
%% Process signals
t=1/FS:1/FS:duration;
dB = zeros(num_mics+1,32769); %

%define filter for signal
B=fir1(40,.1,'high');
B2=fir1(40,.2,'low');

dt=t(2)-t(1);
tau=2e-3:dt:4.5e-3;
R = zeros(num_mics,length(tau));
%Rmax is the index of the maximum of the sample-averaged correlation, for
%each mic and station.
Rmaxind = zeros(num_mics,num_stations);

fprintf('Compiling signals\n')
eval(strcat('s',num2str(ref_mic_id),' =zeros();'));
for m=mic_range
    eval(strcat('s',num2str(m),' =zeros();'));
end

if (strcmp(sta_samp,'Station') == 0)
    num_stations = 1;
end
for station=sta_start:1:num_stations+sta_start-1
    R = zeros(num_mics,length(tau));
    eval(strcat('s',num2str(ref_mic_id),'=[];'));
    for m=mic_range
        eval(strcat('s',num2str(m),'=[];'));
    end
    for samp=1:sam_per_sta
        disp(strcat('Station_',num2str(station),'_Sample_',num2str(samp)));
        switch sta_samp
            case 'Station'
                  filename=strcat(folder,test_series,'Station_',num2str(stati
            on),'_Sample_',num2str(samp),'.mat');
            case 'Data'
                  filename=strcat(folder,test_series,'Data_',num2str(samp),'.
            mat');
            case 'Sample'
```

```
                filename=strcat(folder,test_series,'Sample_',num2str(samp),
            '.mat');
        end
        Data = load(filename);
        for m=[ref_mic_id mic_range]
            % Store data in simple variable
            eval(strcat('s = detrend(Data.AI',num2str(m),'.Data);'));
            s = s / gain(m+mic_array_offset);
            s_low=filtfilt(B,1,s);
            sf(samp,:,m+mic_array_offset)=filtfilt(B2,1,s_low);
            if strcmp(filter,'off')
                sf(samp,:,m+mic_array_offset)=s;
            end
            % Compute Spectra
            if com_spectra == 1
                [p(m+mic_array_offset,:),f] =
pwelch(sf(samp,:,m+mic_array_offset),[],[],[],FS);
                dB(m+mic_array_offset,:) = dB(m+mic_array_offset,:) + (114 +
10*log10(p(m+mic_array_offset,:)/15.925));
            end
            % 1-11: Time Series, 10 ms
            if samp==1
                figure(m+mic_array_offset)
                plot(t*1000,sf(samp,:,m+mic_array_offset))
                xlim([0 10])
                xlabel('Time (ms)')
                ylabel('Pressure (Pa)')
                title({"Unfiltered Dual Hartmann Signal -",strcat(name_case,"
M",num2str(m))})
                savefig(strcat(folder,test_series,"Mic_",num2str(m),"-
Signal_rev1"))
                saveas(gcf,strcat(folder,test_series,"Mic-",num2str(m),"-
Signal_rev1.png"))
            end
        end
    end
    if com_spectra == 1
        dB = dB./sam_per_sta;
        for m=[ref_mic_id mic_range]
            % 12-22: Spectra; Measured Gains
            figure(m+12)
            plot(f/1000,dB(m+mic_array_offset,:))
            xlim([0 30])
            xlabel('Frequency (kHz)')
            if m==ref_mic_id
                ylabel('SPL (dB re 20 \muPa')
            else
                ylabel('SPL (dB re 20 \muPa) at 1.2m')
            end
            title({"Unfiltered Dual Hartmann Spectra -",strcat(name_case,"
M",num2str(m))})
            peakdB(m+mic_array_offset)=max(dB(m+mic_array_offset,:));
            savefig(strcat(folder,test_series,"Mic_",num2str(m),"-
Spectra_rev1"))
            saveas(gcf,strcat(folder,test_series,"Mic-",num2str(m),"-
Spectra_rev1.png"))
        end
```

```
    end
    if com_TOF == 1
        for m=mic_range

Rtest=GCC_sample_ave(sf(:,:,m+mic_array_offset),sf(:,:,ref_mic_id+mic_array_o
ffset),tau,gcc_method, numseg, FS, FS);
            R(m-ref_mic_id,:)=Rtest;
            [Rmax,ind] = max(R(m-ref_mic_id,:));
            Rmaxind(m-ref_mic_id,station) = ind;
            % 23-32: Correlations
            figure(m+22)
            plot(tau*1000,R(m-ref_mic_id,:))
            hold on
            title(strcat(gcc_method," Correlation for M",num2str(m),",
",name_case))
            xlabel('Time Difference (ms)')
            xlim([tau(1)*1000 tau(end)*1000])
            ylabel('Correlation Coefficient')
            plot(tau(Rmaxind(m-ref_mic_id,station))*1000,R(m-
ref_mic_id,Rmaxind(m-ref_mic_id,station)),'ro')
            pause(0.01)
            hold off
            savefig(strcat(folder,test_series,"Mic_",num2str(m),"-
",gcc_method,"_rev2"))
            saveas(gcf,strcat(folder,test_series,"Mic-",num2str(m),"-
",gcc_method,"_rev2.png"))
        end
        for m=mic_range
            delay(m-ref_mic_id,:)=tau(Rmaxind(m-ref_mic_id,station));
        end
        cdelay=delay+tref;
        for m=mic_range
            mediancdelay(m-ref_mic_id)=median(cdelay(m-ref_mic_id,:));
            cdequiv(m-ref_mic_id) = mediancdelay(m-ref_mic_id).*camb./0.0254;
        end

        % 33+: Stations
        figure(station+32)
        plot((mic_range),1000*delay,'ko');
        grid minor;
        xlabel('Microphone Number (M#)')
        ylabel('\tau (ms)')
        title({"Uncorrected Time Delay (Peak) from M1 to M2-
M8,",name_case},'Fontweight','normal');
        ylim([2,4.5]);
        savefig(strcat(folder,test_series,"Allmics-",gcc_method,"_rev1"))
        saveas(gcf,strcat(folder,test_series,"Allmics-
",gcc_method,"_rev1.png"))

save(strcat(folder,test_series,"TOF_",gcc_method,"_rev2"),'cdequiv','mediancd
elay','tref')   % ,'cdequiv_p'
    end
end
```

GCC_sample_ave

```
function [R,ind]=GCC_sample_ave(s1,s2,tau,gcc_method, numseg, L, FS)
```

```
    %FS should be the sampling rate
    %window should be a window of a given length
    %overlap is fixed at 50% for now
    %sample call:
    %[R,maxind]=GCC_sample_ave(s1,s2,tau,'ML',9,L,FS)
    seglen = floor(2*L/(numseg+1));
    for samp=1:size(s1,1)
        [Gxx1(samp,:),f] =
cpsd(s1(samp,:),s1(samp,:),rectwin(seglen),floor(seglen/2),seglen,FS);
        [Gxx2(samp,:),~] =
cpsd(s2(samp,:),s2(samp,:),rectwin(seglen),floor(seglen/2),seglen,FS);
        [Gx1x2(samp,:),~] =
cpsd(s1(samp,:),s2(samp,:),rectwin(seglen),floor(seglen/2),seglen,FS);
    end
    Gxx1sum = zeros(1,length(f));
    Gxx2sum = zeros(1,length(f));
    Gx1x2sum = zeros(1,length(f));

    Gx1x2_array = Gx1x2;
    for samp=1:size(s1,1)
        Gxx1sum = Gxx1sum+Gxx1(samp,:);
        Gxx2sum = Gxx2sum+Gxx2(samp,:);
        Gx1x2sum = Gx1x2sum+Gx1x2(samp,:);
    end
    Gxx1 = Gxx1sum/size(s1,1);
    Gxx2 = Gxx2sum/size(s1,1);
    Gx1x2 = Gx1x2sum/size(s1,1);
    COH2 = Gx1x2.*conj(Gx1x2)./(Gxx1.*Gxx2);
    COH2 = COH2';

    switch gcc_method
        case 'SCC'
            W = ones(length(Gxx1),1);
        case 'PHAT'
            W = 1./abs(Gx1x2');
        case 'Roth'
            W = 1./Gxx1';
        case 'SCOT'
            W = 1./sqrt(Gxx1'.*Gxx2');
        case 'Wiener'
            W = COH2;
        case 'ML'
            W = COH2./(abs(Gx1x2').*(1-COH2));
        case 'PHAT_Wiener'
            W = COH2./abs(Gx1x2');
        case 'Roth_Wiener'
            W = COH2./Gxx1';
        case 'SCOT_Wiener'
            W = COH2./sqrt(Gxx1'.*Gxx2');
        case 'SCOT_ML'
            W = COH2./(sqrt(Gxx1'.*Gxx2').*(1-COH2));
        case 'Roth_ML'
            W = COH2./(Gxx1'.*(1-COH2));
        case 'Rev_Roth'
            W = 1./Gxx2';
    end
    R = zeros(1,length(tau));
```

```
for samp=1:size(s1,1)
    Coeff = Gx1x2_array(samp,:).*W';
    summatrix = ((Coeff.' * ones(size(tau))).* exp(1i.*2.*pi.*f * tau));
    %Find correlation function
    R=R+real(sum(summatrix,1));
end
R=R/size(s1,1);
R=R/max(R);
% Find TOF index
[~,ind]=max(R);
```